Technical University of Hamburg-Harburg, Faculty of Electrical Engineering
Helsinki University of Technology, Faculty of Electrical Engineering

Clemens Icheln

THE CONSTRUCTION AND APPLICATION OF A GTEM CELL

Master's Thesis

Erklärung

Hiermit erkläre ich, daß ich die hier vorliegende Arbeit selbständig und ohne fremde Hilfe angefertigt und keine anderen als die angeführten Hilfsmittel verwendet habe.

Helsinki, den

Author: Clemens Icheln
Subject: The construction and application of a GTEM cell

Date: November 1 1995 **Number of pages:** 53

Made at the Radio Laboratory of the Faculty of Electrical Engineering of the HUT in co-operation with the Research Area of Measurement Engineering of the Faculty of Electrical Engineering of the TUHH.

Supervisors:
Prof. Dr.-Ing. Jan-Luiken ter Haseborg (TUHH)
Assoc. Prof. Dr.-Tech. Pertti Vainikainen (HUT)

Abstract:
The GTEM (Gigahertz Transversal Electromagnetic Mode) cell is a flared transmission line that is operated in the TEM mode to simulate a free space planar wave. It can be used for radiated susceptibility tests as well as for measurements of radiated emissions of electronic equipment at frequencies from dc up to over 1 GHz.
In this paper the theory, the design and the construction of a 2.2 m long GTEM cell are described. Special attention is directed to the design of the apex and the termination section. Due to the wideband matching of the cell the return loss is better than 16 dB below 80 MHz and better than 20 dB from 80 – 2600 MHz. Hereby a uniform field inside a defined testing volume is obtained, that allows EMC tests of equipment with a size of up to 23 cm x 17 cm x 10 cm.
As an application the radiation pattern of a small antenna is evaluated by means of the GTEM cell and the results are compared to those obtained in an anechoic room. The results indicate the possibility for using the GTEM for determining certain properties of antennas like the gain or the 3 dB beamwidth without the usually used costly anechoic rooms. Restrictions of the antenna measurements are pointed out.

Keywords: GTEM cell, Electromagnetic Compatibility, Transverse Electromagnetic Mode, Antenna Measurements

Autor: Clemens Icheln
Thema: Die Konstruktion und Anwendung einer GTEM Zelle

Datum: 1. November 1995 **Seitenzahl:** 53

Angefertigt im AB Hochfrequenztechnik der Fakultät für Elektrotechnik der HUT in Verbindung mit dem AB Meßtechnik der Fakultät für Elektrotechnik der TUHH

Betreuer:
Prof. Dr.-Ing. Jan-Luiken ter Haseborg (TUHH)
Assoc. Prof. Dr.-Tech. Pertti Vainikainen (HUT)

Abstract:
Die GTEM (Gigahertz Transverse Electromagnetic Mode)-Zelle ist ein trichterförmig erweiterter TEM-Leiter. Mit der GTEM-Zelle kann die elektromagnetische Verträglichkeit (EMV) einer elektrischen Einrichtung gemessen werden. So kann die GTEM-Zelle sowohl zum Testen der strahlungsgebundenen Störfestigkeit als auch für Messungen von Störausstrahlung benutzt werden, beides in einem Frequenzbereich von Gleichstrom bis weit über 1 GHz.
In der vorliegenden Arbeit wird die Theory, die Entwicklung und der Aufbau einer GTEM-Zelle beschrieben, sowie die anschließende Kalibrierung und Anwendung.
So wird u.a. die Abstrahlcharakteristik einer elektrisch kleinen Antenne gemessen und die Ergebnisse mit denen entsprechender Messungen in einer Schirmkabine verglichen.

Stichworte: GTEM cell, Electromagnetic Compatibility, Transverse Electromagnetic Mode, Antenna Measurements

Preface

This diploma thesis has been made in the Radio Laboratory of the Helsinki University of Technology in co-operation with the Arbeitsbereich Meßtechnik of the Technical University Hamburg-Harburg. I want to thank the two professors, who made this co-operation possible, i.e. Professor J.-L. ter Haseborg for being the supervisor at my home university and Associate Professor Pertti Vainikainen for his supervision of the thesis at the HUT. The instruction by Pertti Vainikainen was a great support during the completion of this work.

Furthermore I want to thank the staff of the radio lab for the support during my work. Special thanks to Matti Fischer and Tomas Sehm for always being ready to help me with technical problems and to Päivi Haapala and Pauliina Erätuuli who made their results of the field pattern measurements of the $\lambda_G/4$ patch antenna available to me.

Many thanks as well to Lauri Puranen at STUK for making the calibrated field probe available to me and to Antero Koivisto with whom I have exchanged several articles.

Ich möchte mich auch bei Lorenz Schmuckli bedanken, der mir beim eigentlichen Bau der Zelle sehr oft weitergeholfen hat.

Und zu guter Letzt moechte ich noch meinen Hamburger Freunden Gernot Neppert, Skandia Schenk, Imke Staats, Werner Walczak und Stefan Woitschig für ihre 'mentale' Unterstützung, als sie mich hier, fern von meiner Heimatstadt besuchten, danken.

Espoo,

Table of contents

List of abbreveations

dc	Direct Current
EMC	Electromagnetic Compatibility
EUT	Equipment Under Test
GTEM	Gigahertz Transverse Electromagnetic Mode
OATS	Open Area Test Site
RCTL	Rectangular Coaxial Transmission Line
RF	Radio Frequency
TDR	Time Domain Reflectrometry
TEM	Transverse Electromagnetic Mode

List of symbols

a	width of the outer conductor
a_{cell}	total width of the cell
a_{near}	width of the cell at the near end of the testing volume
AF	antenna factor
c_0	speed of light in vacuum
C	capacitance
d	height of the outer conductor
d_1	height of the outer conductor at the beginning of the apex
d_2	height of the outer conductor at the end of the apex
d_{cell}	total height of the cell
E	electric field strength
E_{max}	maximum attainable electric field strength
E_n	normal component of the electric field strength
E_{nom}	nominal field strength inside the testing volume
g_n	auxiliary variable
G_a	gain of an antenna
h	distance between the bottom outer conductor and the center conductor
h_2	h at the end of the apex
h_{near}	h at the near end of the testing volume
h_{far}	h at the far end of the testing volume
i	auxiliary variable
K	auxiliary variable
l_0, l_1	integration paths around center conductor
l_{apex}	length of the apex
l_{cell}	total length of the GTEM cell
l_{tooth}	length of a tapered tooth
n	auxiliary variable

P	power
P_{in}	input power of the GTEM cell
P_{max}	maximum input power of the GTEM cell
Q	charge
r	radius
R	resistance
Δs	difference in length of the conductors in a TEM cell
Δt	difference in travel time of waves inside a TEM cell
t	time
u	thickness of the center conductor
U	voltage
U_{inner}	voltage at center conductor
U_{outer}	voltage at outer conductor
v	width of a tapered tooth
V_{1n}, V_{2n}	auxiliary variables
w	width of the center conductor
w_1	width of the center conductor at the beginning of the apex
w_2	width of the center conductor at the end of the apex
x	horizontal coordinate
y	vertical coordinate
z	longitudinal coordinate
Z	characteristic impedance
Z_L	impedance of a transmission line load
α	angle about y-axis
ϵ_0	permittivity of free space
ϵ_c	complex permittivity
ϵ_r	relative permittivity
ϵ'	real part of the complex permittivity
ϵ''	imaginary part of the complex permittivity
ϕ	potential
Γ	power reflection coefficient
λ	wavelength
λ_G	wavelength in substrate
ω	angular frequency
ϱ	charge density

1 Introduction

The Electromagnetic Compatibility (EMC) of an electrical device is its capability to operate safely in an electromagnetic environment without interfering with this environment in an inadmissable way.

From 1996 all electronic products that are sold in the European Union common market have to be tested for their electromagnetic compatibility (EMC). Standard EMC tests include (a) susceptibility tests, where different radiated and conducted disturbances are applied on a device, and (b) measurements of radiated and conducted emissions of a device. The radiated susceptibility tests and emission measurements require reproducible measuring methods, some of which are mentioned here:

An open area test site (OATS) is characterised by a large ground screen and the absence of other conducting surfaces surrounding the equipment under test (EUT). Antennas are used to generate and to measure the fields.

It is rather difficult to establish an OATS without interfering with existing external electromagnetic fields like the increasing amount of radio frequency transmissions from civil communication systems. The external sources cause errors in the measurements of radiated emissions as well as they are affected by the fields that are generated in susceptibility tests.

Open field measurements are due to the setup useful only at frequencies above about 30 MHz. OATSs are used for the calibration of antennas as well as for EMC testing because they provide a straightforward approach to evaluating the EMC characteristics of electronic equipment.

Anechoic rooms have been used for electromagnetic compatibility measurements in an electromagnetic isolated environment according to international standards (e.g. IEC 1000-4-3). Electromagnetic fields are established and measured by means of antennas. The walls of anechoic rooms are covered with RF absorbers to simulate a free space environment. However, the absorption is usually not perfect so that resonances and reflections may introduce errors to both susceptibility tests and emission measurements. Other problems are the high costlyness of the large amount of absorbing material and the high input power that it necessary to establish e.g. a field strength of 10 V/m at 3 m distance from the antenna.

In 1974 M.L. Crawford described the TEM (Transverse Electromagnetic Mode) cell (or so called Crawford Cell) [1]. It is an expanded planar transmission line operated in the TEM mode to simulate a free space plane wave. As it is a mobile shielded enclosure it can be handled much easier than any of the previous test setups. It can be used for radiated susceptibility tests and emission measurements up to a frequency of about 500 MHz depending on the mechanical dimensions of the cell (see chapter 2).

An improved absorber-loaded TEM cell was developed [2] but still the highest achievable frequency was far below 1 GHz. Nevertheless this gave the idea for a new TEM cell type to meet the demand for EMC measurements at even higher frequencies.

The GTEM (Gigahertz Transversal Electromagnetic Mode) cell was introduced in 1987 by D. Königstein and D. Hansen [3] and overcame many limitations of the previous TEM cells. It is based on a TEM-cell anechoic-chamber hybrid concept which means that it is an expanded transmission line operated in the TEM mode and terminated with a broadband hybrid load [4]. Due to this it can be used for radiated susceptibility tests as well as for emission measurements for frequencies from dc up to 1 GHz or even higher.

The aim of this work is the construction of a GTEM cell which allows testing the radiated EMC properties of small electronic equipment according to the international standards for radiated EMC measurements, e.g. IEC 1000-4-3 [5] and EN 55 022 [6].

As the cell that is built in this work will be used not only for research but also for demonstration purposes for example within lectures one of the main specifications for the cell is the portability. This requirement restricts the overall dimensions and weight of the cell and therefore leads to a relatively small cell when compared to the commercial ones.

In this thesis at first the concept behind the TEM cells and in particular the GTEM cell is described in chapter 2. The properties of the GTEM cell are discussed.

In chapter 3 the design and the construction of the GTEM cell developed and build in this work are described. An important aspect of the termination is to have a low reflection coefficient in the described frequency range. Therefore the two components of the termination, i.e. the current termination and the wave termination are discussed, both in theory and through measurements during the evaluation of the cells properties.

In chapter 4 the practical realization of radiated susceptibility tests and emission measurements with a GTEM cell is explained in detail. Results from measurements done with this GTEM cell are described. As one application the field pattern of a small antenna is evaluated by means of the GTEM cell and compared to results obtained in an anechoic room.

2 Theory

The principle of the GTEM cell is the generation of a uniform field inside a shielded environment by operating an expanded transmission line in the TEM mode. This is quite similar to the idea behind the former TEM cell, so first a brief look is taken at the TEM cell. Opposed to that the differences and advantages of the concept of the GTEM cell are explained.

2.1 Principle of TEM cells

The TEM cell was designed based on the concept of an expanded planar transmission line operated in a TEM mode to simulate a free space planar wave for susceptibility testing.

The TEM cell is mainly a section of a rectangular coaxial transmission line with a flat and wide center conductor and tapered ends acting as transitions to adapt to standard 50 Ω coaxial connectors (see figure 2.1).

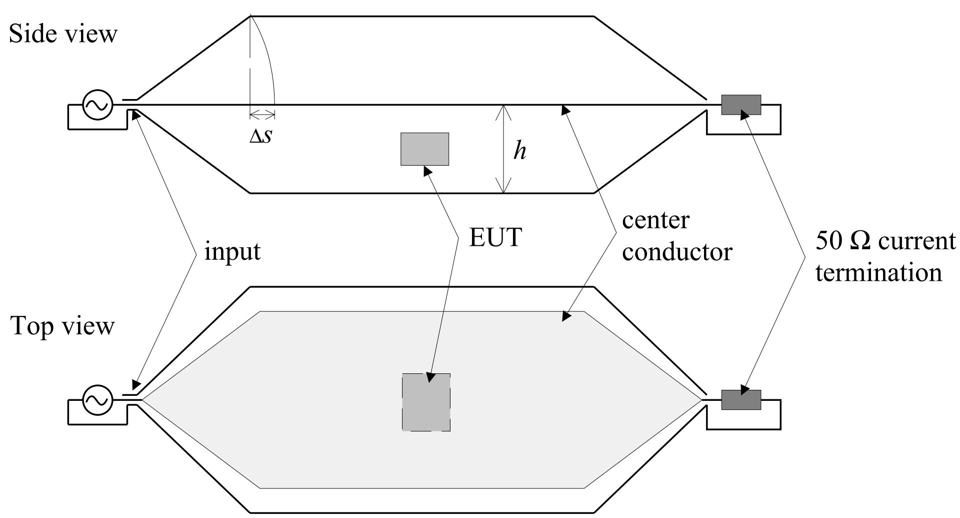

Figure 2.1: *Schematic diagram of the TEM cell with the center conductor and the tapered ends. The maximum height of the EUT is typically one third of the distance h. Δs denotes the difference in length of the conductors which limits the usable frequency range.*

To minimize reflections and thus also the standing-wave ratio the cell usually has a characteristic impedance of 50 Ω along its length. The size of an EUT is typically restricted to one third of the height h because the EM field is sufficiently uniform only within that region. Furthermore, for larger equipment the effect of the equipment itself on the field strength would be too large as to get reliable results. The well isolated TEM cell neither contributes to nor is affected by any external interference.

In susceptibility tests the power is fed through one input of the TEM cell. From there electromagnetic waves propagate spherically in the tapered part of the cell whereas in the main volume of the cell the wave front changes to a planar one. Therefore in the middle part where the EUT will be situated the field strength is constant along the longitudinal extension unless the presence of an EUT alters the field e.g. with possible conductive or dielectric components. The electromagnetic waves as well as the current in the center conductor are terminated by a matched load impedance at the second input of the cell. An advantage over anechoic rooms is the elimination of antennas for establishing the EM fields. In order to reach a certain field strength at the position of the EUT the necessary input power is much lower for a TEM cell than the input power of the antennas in an anechoic room.

As the TEM cell serves as its own transducer it can very well be used for emission tests. Again the elimination of antennas is an advantage over OATSs and anechoic rooms. When carrying out emission measurements one or both inputs of the cell are used for monitoring the output power as a result of emissions from the tested equipment. When using both inputs one obtains a relative phase information which is useful if there is directivity in the emissions. As the emission measurements are performed by monitoring the output voltage across the input(s) of the cell and not by determining the radiated fields directly with help of antennas, methods have been set up to correlate the data obtained from the TEM cell measurements to the standard OATS measurements [7], [8] as for meaningfully comparing results.

A clear drawback of the TEM cell is the limited useful frequency range due to the cell consisting of three differently shaped parts. Due to the corners of the transitions the lenght of the inner and outer conductor differs by Δs (see figure 2.2). So along the outer conductor the travel time for a wave is longer by $\Delta t = \frac{\Delta s}{c_0}$. These field distortions give rise to higher mode propagation and thus affect the uniformity of the field inside the cell increasingly at higher frequencies. The highest frequency to use the cell depends mainly on the angle at the transition from the middle part to the tapered ends and thus on the opening angle of the two tapered parts.

The size of the cell is another limiting factor as the cell shows cavity effects like resonances at frequencies at which the dimensions of the cell are about half the wavelength. According to IEC 1000-4-3 [5] a TEM cell can therefore be typically used only up to about 200 MHz.

To increase the upper frequency limit of the TEM cell with respect to the cavity effects absorbing material can be placed on the walls [2] in order to minimize resonances and reflections. Thereby the useful frequency range can be extended but the upper frequency limit is still below 1 GHz.

2.2 The GTEM cell

The development of the GTEM cell in 1987 [3] made EMC measurements possible at frequencies from dc up to 1 GHz or even higher which was a large progress against the limited usable frequency range of the TEM cell.

The new idea behind the GTEM cell was to avoid the corners that are the main reason for the limitations of the frequency range of the TEM cell. Therefore the main volume of the GTEM cell is only one section of a flared rectangular transmission line (see figure 2.2). That means the length of inner and outer conducter is equal and thus the travel time along each conductor is equal. This property is also an important factor for pulse type measurements, as the dispersion of the pulse is minimized.

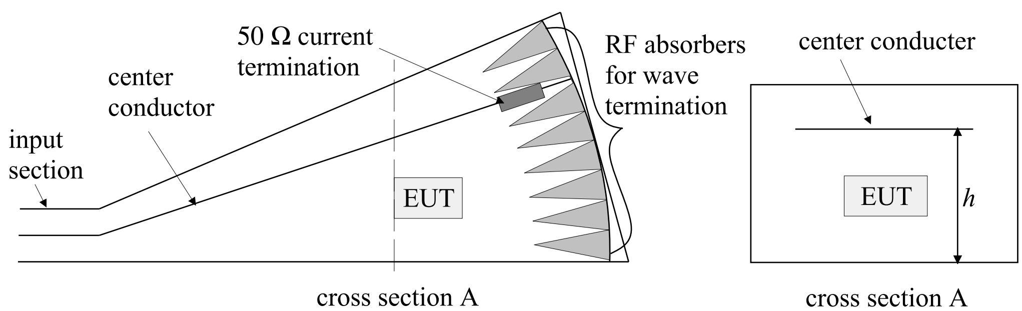

Figure 2.2: *Schematic diagram of a GTEM cell. It is a flared rectangular transmission line with the center conductor situated above the center line. The height of an EUT is restricted to $\frac{1}{3}$ of the distance h between bottom outer conductor and center conductor.*

Usually resonances arise in a closed cavity. Due to the flared shape this is not the case in a GTEM cell. The GTEM is like the former TEM cell well isolated and therefore neither contributes to nor is affected by any external interference.

The cell typically has a detachable input section, a so called apex. In the tip a standard 50 Ω coaxial connector is mounted. In the input section then the transition from the standard 50 Ω coaxial connector to the asymmetric rectangular waveguide with a flat center conductor is done.

The cell opens with an angle of 20° in the vertical plane and 30° in the horizontal plane respectively. Hence, the cross-sectional dimensions of the rectangular waveguide are a height to width ratio of 2 to 3. The center conductor is vertically offset to increase the usable test volume as opposed to a symmetric configuration. It is typically situated at three quarters of the cell height. The effect of this assymmetry on the field uniformity inside the volume below the center conductor is negligible against the advantage from the increased test volume. This will be discussed in more datail in chapter 4.

To achieve a characteristic impedance of 50 Ω the ratio of the width of the center conductor to that of the outer conductor is 0.636 according to the patent [9]. So far there are no closed form equations to calculate the impedance of such a geometry, so the given value is considered approved by numerical methods and by measurements. In section 2.3 two methods will be given to approximate the impedance of the given geometry numerically.

A testing volume is defined, within which the variations of the field strength are within a defined limit. This is to ensure the reliability and repeatability of measurements. For susceptibility testing an electronic device is placed in the testing volume and a CW- or pulse-generator is connected to the input of the cell according to the requirements. The propagation mode is TEM again but the waves are in this case slightly spherical. Due to the small opening angle they are very close to free space planar waves. Therefore the measurement procedure with a GTEM cell can be very well compared with standard measurements like in anechoic rooms.

The field uniformity inside the testing volume depends very much on a low level of reflections from the rear end of the cell. In order to absorb most of the energy that reaches the rear end a wideband matched termination is assembled at the rear wall. A closer look at this termination section is taken in section 2.4.

The field strengh inside the cell is decreasing in a $1/r$ manner along the longitudinal direction. This is due to the fact that the cell is a wedge from a sphere with a solid angle, i.e. the $1/r$ behaviour is consistent with a spherical wave.

The nominal field strength in the testing volume typically refers to the field strength at the center of the testing volume which is approximately the fraction of the voltage and the distance between inner conductor and bottom outer wall $E = \frac{U_{inner} - U_{outer}}{h}$. The respective input power is given by the input voltage squared devided by the characteristic impedance of the transmission line $P = \frac{U^2}{Z}$ and thus the necessary input power as a function of a desired field strength at the position of the EUT is

$$P = \frac{(E \cdot h)^2}{Z}. \tag{2.1}$$

The field strength at the position of the EUT is

$$E = \frac{\sqrt{P \cdot Z}}{h}. \tag{2.2}$$

So the field strength is a function of the input power and the distance h from the bottom outer to the center conductor. In figure 2.3 the nominal field strength in the testing volume is plotted against h for different values of P with a characteristic line impedance of $Z = 50\ \Omega$.

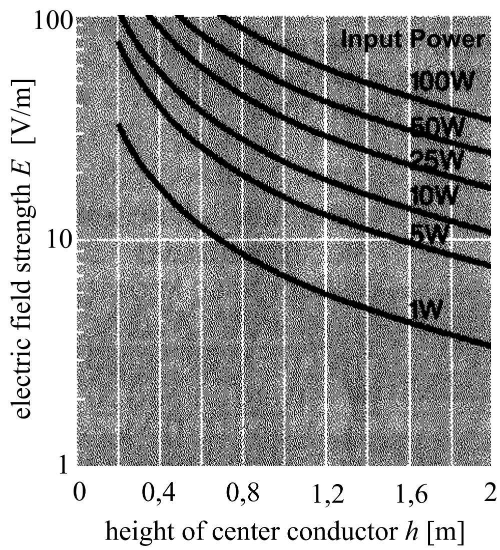

Figure 2.3: *The calculated nominal field strength in the center of the volume below the center conductor as a function of input power and distance h between the bottom outer conductor and the center conductor.*

A nominal field strength in the testing area of 10 V/m will meet most requirements for EMC measurements. For a small cell with a distance $h = 0.5$ m at the testing volume a nominal field strength of 10 V/m can be achieved with an input power of $P = 0.5$ W according to (2.2). Even for larger cells the input power is much less than the necessary input power for susceptibility measurements performed in anechoic rooms, where the EUT is typically situated 3 or 10 m from the transmitting antenna.

For emission measurements the input of the GTEM cell is connected to the measuring equipment to monitor the output voltage as a result of emissions from the tested equipment inside the cell.

It can be assumed that only the power directed towards the input along the longitudinal axis of the cell will be measured at the input. In any other direction than towards the input the waves arising from the EUT can not propagate or are terminated by the hybrid termination in the rear end. This property will be shown by measurements of the field pattern of a small antenna in chapter 4.

In the reference environment for radiated emission measurements, which is typically free space or an OATS, the actual electric and magnetic field strength in every direction is obtained through antennas at a certain distance. The results from a GTEM emission measurement consisting of output voltage data must be correlated with these environments if data is to be meaningfully compared. That procedure will be explained in chapter 4.

Hence, the GTEM cell can be used for susceptibility testing as well as for emission measurements for frequencies from dc up to several gigahertz due to the broadband hybrid termination and the fact that there are no frequency limitations from mechanical dimensions as for the conventional TEM cell.

2.3 Characteristic impedance

The GTEM cell is an expanded transmission line operated in the TEM mode so the characteristic impedance of 50 Ω must be ensured to avoid reflections that would cause higher order modes. For the design of the cell the dependence of the characteristic impedance on the geometrical dimensions must be known. As there are no closed formulas for the characteristic impedance of an asymmetric rectangular transmission line, numerical methods are necessary.

In this section two different ways how to numerically approximate the characteristic impedance of a rectangular transmission line are described and compared. The geometry of a GTEM cell that is given in the patent for the GTEM cell [9] will be verified with help of those two methods. Furthermore, the influence of changes in the geometry of such a transmission line on its characteristic impedance is illustrated.

Apart from the approximation within the numerical method itself another approximation is made when the small opening angle is neglected. This is done because then the mode of propagation in the GTEM cell can be considered an ideal TEM mode and the field pattern of the TEM mode can be modelled by an electrostatic field case. Thus an approach for electrostatic fields in an untapered rectangular coaxial transmission line is used to approximate the characteristic impedance of the GTEM cell.

The first method, which is given in [10], uses the variational principle for approximating the capacitance of a rectangular coaxial transmission line with an infinitely thin and vertically offset center conductor as shown in figure 2.4.

The Poisson's equation describes the relation between the potential distribution ϕ in the cross section and the charge distribution $\varrho(x,y)$

$$(\frac{\partial^2}{\partial x^2}+\frac{\partial^2}{\partial y^2})\phi(x,y)=\frac{1}{E}\varrho(x,y). \tag{2.3}$$

The following are the boundary conditions due to the outer conductor

$$\phi(-\tfrac{1}{2}a,y)=0, \tag{2.4}$$

$$\phi(\tfrac{1}{2}a,y)=0, \tag{2.5}$$

$$\phi(x,0)=0, \tag{2.6}$$

$$\phi(x,d)=0. \tag{2.7}$$

The continuity condition due to the conductor at $y=h$ which is considered infinitely thin $(u\to 0)$ is

$$\frac{\partial}{\partial y}\phi(x,h-0)=\frac{\partial}{\partial y}\phi(x,h+0)-\varrho(x,h), \tag{2.8}$$

where $h+0$ and $h-0$ denote an infinitely small offset above and below the center conductor respectively. $\varrho(x,h)$ is the charge density on the conductor.

Green's function gives at (x,y) the potential caused by a unit charge situated at the position (x_0,y_0). Therefore it is a solution to the problem similar to (2.3):

$$(\frac{\partial^2}{\partial x^2}+\frac{\partial^2}{\partial y^2})G(x,y|_{x_0,y_0})=\frac{1}{E}\delta(x-x_0)\delta(y-y_0). \tag{2.9}$$

When the Green function is found, the potential due to the charge distribution on the conductor surface is given with help of the superposition principle, which is expressed by the integration along the surface of the center conductor denoted by l_0 (see figure 2.4) as

$$\phi(x,y)=\int G(x,y|_{x_0,y_0})\varrho(x_0,y_0)dl_0. \tag{2.10}$$

When denoting the boundary of the cross section by l_1 according to [10] the capacitance per unit length for a transmission line is given by

$$C=\frac{\left[\int \varrho(x,y)dl_1\right]^2}{\int\int \varrho(x,y)G(x,y|_{x_0,y_0})\varrho(x_0,y_0)dl_0dl_1} \tag{2.11}$$

when maximized by a suitable choice for the charge density as a trial function. This procedure of calculation is called the variational principle.

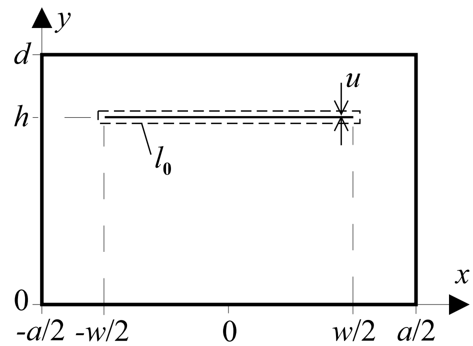

Figure 2.4: *The cross section of a rectangular coaxial transmission line with a thin and vertically offset center conductor.* l_0 *denotes the integration path along the surface of the center conductor.*

As a trial function for the charge density in the center conductor a function has been chosen that shows a high value at the edges when compared to the center of the inner conductor

$$\varrho_{trial}(x) = 1 + K|\frac{2x}{w}|^3. \tag{2.12}$$

According to [10] Green's function in (2.11) is expanded in a Fourier series in order to finally transform (2.9) in a set of ordinary differential equations. These are solved by a linear combination of sinusoidal and hyperbolic sinusoidal functions.

This procedure leads finally to an approximation for the line capacitance per unit length in the following easy-to- compute form:

$$C = \frac{2\epsilon_0(1+\frac{1}{K})^2}{\frac{a^2}{w^2}\sum\limits_{n=1}^{\infty}(V_{1n}+KV_{2n})^2 g_n}, \tag{2.13}$$

where K, V_{1n}, V_{2n} and g_n are subtitutes for the following expressions:

$$K = -\frac{\sum\limits_{n=1}^{\infty}(4V_{2n}-V_{1n})V_{1n}g_n}{\sum\limits_{n=1}^{\infty}(4V_{2n}-V_{1n})V_{2n}g_n}, \tag{2.14}$$

$$V_{1n} = \frac{4}{n\pi}\sin(\tfrac{n\pi}{2})\sin(\tfrac{n\pi w}{2a}), \tag{2.15}$$

$$V_{2n} = \frac{2w}{a}\sin(\tfrac{n\pi}{2})\left(\frac{\sin(\frac{n\pi w}{2a})}{(\frac{n\pi w}{2a})} + \frac{3}{(\frac{n\pi w}{2a})^2}\left[\cos(\tfrac{n\pi w}{2a}) - \frac{2\sin(\frac{n\pi w}{2a})}{(\frac{n\pi w}{2a})} + \frac{\sin^2(\frac{n\pi w}{4a})}{(\frac{n\pi w}{4a})^2}\right]\right) \tag{2.16}$$

and

$$g_n = \frac{\sinh(\frac{n\pi h}{a})\sinh(\frac{n\pi(d-h)}{a})}{n\pi\sinh(\frac{n\pi h}{a} + \frac{n\pi(d-h)}{a})}. \tag{2.17}$$

The characteristic impedance is then proportional to the reciprocal of the capacitance:

$$Z = \frac{1}{c_0 C} \tag{2.18}$$

where c_0 denotes the speed of light on vacuum.

The program Mathematica has been used for several different geometries to evaluate the characteristic impedance according to the given equations (2.13) to (2.18). The sums though were evaluated only up to $n = 100$, because for a limit above this the results of the sums do not change in a remarkable way.

Figures 2.5 and 2.6 illustrate the influence of the width and the vertical position of the center conductor respectively on the charateristic impedance.

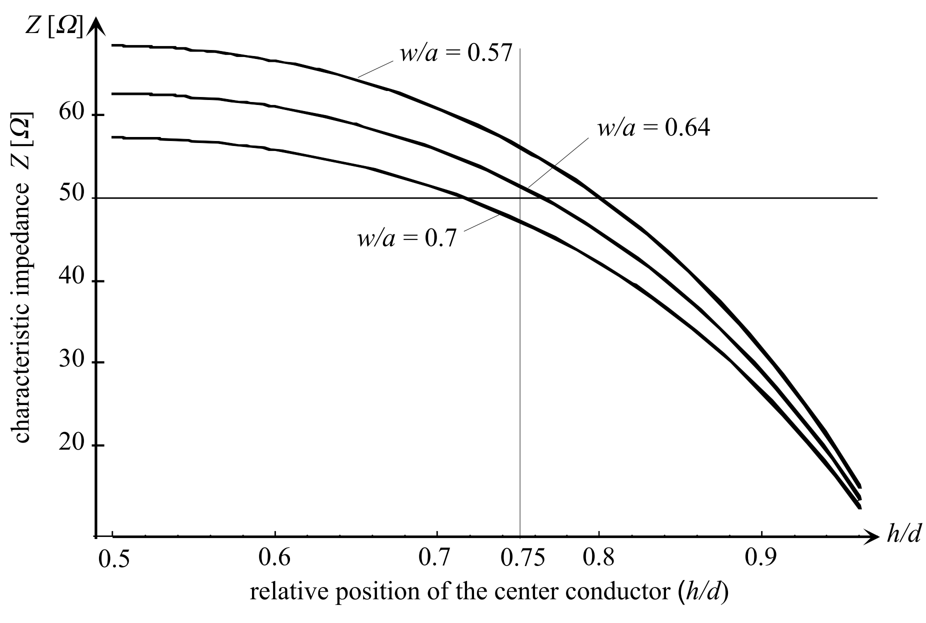

Figure 2.5: *The characteristic impedance related to the vertical position of the center conductor for three different values for its width.*

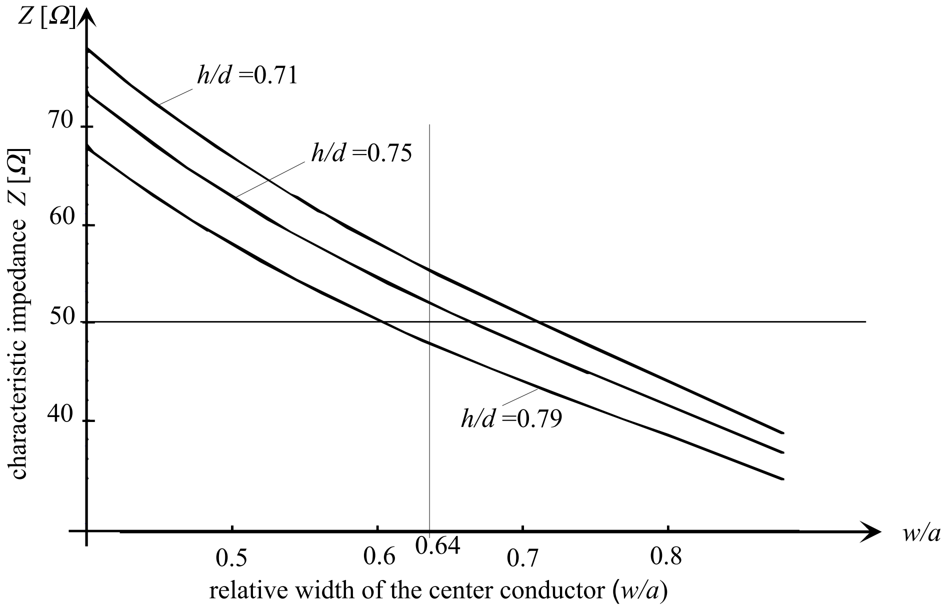

Figure 2.6: *The characteristic impedance related to the width of the center conductor for three different values for its vertical position.*

For a width ratio of $w/a = 0.636$ this numerical approach results in an impedance of 52 Ω. Compared to the nominal impedance of 50 Ω the result is by 2 Ω too high but still this method gives an idea about the behaviour of the characteristic impedance as a function of the geometry.

A finite element method system called Quickfield (Students' version 2.3 with a maximum of 500 nodes), that evaluates electrostatic fields in two-dimensional structures, has been used as an alternative to the variational method. Nevertheless the TEM mode is again modelled by electrostatic fields as the same approximations are made as for the tapering of the transmission line.

With Quickfield a characteristic impedance of 50.5 Ω was calculated. This result is very close to the nominal characteristic impedance of 50 Ω and the calculation time on a common 386 personal computer is about 1 minute. Furthermore, Quickfield can easily produce very usefull figures, e.g. of the cross-sectional field pattern or curves of the field strength along a surface. Therefore Quickfield is used for several calculations during the design of the cell.

Still it is rather time intensive to edit the geometry with the Quickfield program. So in some cases where the characteristic impedance has to be calculated it is easier to use the above described variational principle as changes in the geometry can be easily implemented in variables.

2.4 Hybrid termination

Due to the difference in the concepts for the former TEM cell and the GTEM cell a hybrid concept has to be used for the termination in the rear end of the cell.

In the TEM cell only distributed currents in the center conductor have to be terminated which is sufficiently done by a concentrated 50 Ω load at the input connector. In a GTEM cell a termination has to be established in order to simulate a wideband matched load for the entire used frequency range. However, the matching can not be perfect.

Therefore the aim is a low value for the reflection coefficient of the termination in order to minimize the effect of standing waves on the field uniformity inside the testing volume. The hybrid concept which meets this requirement is described in this section.

For terminating the current in the center conductor at frequencies up to some megahertz a single 50 Ω resistor connecting the center conductor to the rear wall would sufficiently act as a matched load. The width of the center conductor though does not allow a connection to just one resistor, because the capacitive and inductive effects would cause reflections at the connection to the rear wall for higher frequencies. In principle a large number of parallel resistors between center conductor and rear wall could minimize those effects.

At frequencies, where $\lambda/2$ is smaller than the cross-sectional dimensions of the cell, the waves start propagating as well in higher modes than in the TEM mode. The higher mode propagation in a GTEM cell is analysed in [11] and [12]. E.g. at a distance from the feed point of $z = 1.2$ m in the volume below the center conductor the TE_{10} mode, which is the first higher order mode, is entering into propagation at about 200 MHz. According to [11] at 1 GHz and at $z = 1.2$ m about 30% of the power has been transfered from the TEM mode to higher modes. The higher order modes can not be terminated by the resistors as they are waveguide modes. In order to terminate those waveguide modes an arrangement of suitable pyramidal RF absorbers has to be assembled at the rear wall. The RF absorbers should have a sufficient return loss at frequencies down to 500 MHz or even down to 200 MHz.

This means there is a certain frequency band in which a crossover from TEM to waveguide propagation takes place and therefore a crossover from current termination to wave termination is necessary. In that intermediate frequency band both parts are not completely effective and only the combination leads to an acceptable reflection coefficient. This must be well considered when designing the termination of the GTEM cell.

2.4.1 Current termination

The resistive termination has to have a high return loss up to frequencies of at least 200 MHz. For the design of such a resistive termination two main aspects have to be taken into account.

The current distribution in the center conductor is typically considered by directly adapting the values of the parallel termination resistors to the current distribution in the center conductor. The number of parallel resistors has an effect on the quality of the termination (see figure 2.8). Similar to the case of the characteristic impedance the current distribution can be approximated with help of numerical methods.

The second aspect is the high conductivity of the lossy absorbers. Towards the rear wall the absorbers fill an increasing part of the cross section. This increases the distributed capacitance of the transmission line and thus the characteristic impedance of the cell is decreasing towards the rear end. A compensation of this effect with help of a certain additional configuration of the current termination section is necessary in order to keep the characteristic impedance at a constant level of about 50 Ω.

In theory this problem could be treated in the following way:

According to the third Maxwell equation the charge Q inside a volume V is given by

$$Q = \oint_V \epsilon_0 \epsilon_c E dV \tag{2.19}$$

In this case the permittivity $\epsilon_c = \epsilon' - j\epsilon'' = \epsilon_0\epsilon_r + \frac{\sigma}{j\omega}$ is a complex number as the absorbers consist of a lossy material. The value of the relative permittivity ϵ_r and the conductivity σ of the absorber material can usually not be easily determined (unless given by the manifacturer). Furthermore, neither the field distribution $E(x,y)$ nor the distribution of the permittivity $\epsilon(x,y)$ within the cross section can be easily calculated, as the pyramidal absorbers fill only parts of the cross section. So accurately modelling the influence of the absorbers on the characteristic impedance is not a very practical way. It will be shown in chapter 3, that a simpler approach will give reasonable results.

For the realization of an appropiate current termination in practice there are mainly two basic concepts. Both approaches can make the current termination effective up to a frequency of about 200 to 500 MHz.

(a) A two-dimensional network of resistors. In the longitudinal direction an increasing level of resistance within the network compensates the increasing distributed line capacitance and in the horizontal direction the resistive distribution adapts to the current distribution in the center conductor. The overall resistance of the network is 50 Ω. This concept is considerably cost intensive due to the large number of resistors.

(b) Tapering the center conductor towards the rear wall in the section where the absorbers are situated. The decreasing width of the center conductor should then compensate the increasing influence of the RF absorbers and yield in a constant characteristic line impedance. Connecting only one tooth to the rear wall by a 50 Ω resistor brings up the same problems due to the geometry as mentioned above for a single-resistor termination. So in the termination section the center conductor is split into several teeth. The tapering of the teeth should then at the same time minimize the reflections that arise from a change in the geometry of the center conductor.

In the patent of the GTEM cell [9] the concept for the current termination consists of three equal parallel resistors connecting the center conductor to the rear wall while the center conductor shows a special tapering towards the rear wall where the RF absorbers are arranged. In the plane where the tips of the absorber pyramids are situated, the center conductor is split into three teeth which taper towards the rear wall, where the resistors are assembled.

The initial width of those teeth adapt to the current distribution in the center conductor. The tapering minimizes the effect of the RF absorbers on the characteristic impedance. The teeth are connected to the rear wall by equal resistors resulting in a parallel resistance of 50 Ω.

In the papers [13] and [14] the current termination is based on a larger number of teeth while the teeth are all of the same width and connected to the rear wall by discrete resistors (see figure 2.7).

The current distribution in the center conductor is considered in the distribution of different parallel resistors. The influence of the RF absorbers is considered in the tapering of the teeth. The parallel resistors yield in an overall load resistance of 50 Ω.

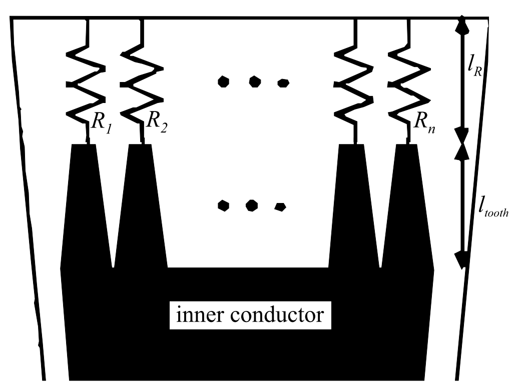

Figure 2.7: *The current termination section in the rear of the cell. The center conductor is connected to the rear wall via a number of teeth each of them followed by a resistor with a resistance value adapting to the current distribution in the center conductor.*

This approach is not used in this work but here is a brief look at its performance (according to [13]) to have a possibilty to compare the performance of the method used in this work which is the above mentioned three-teeth approach.

In [13] a large GTEM cell with a maximum center conductor width of about 3 m is considered. From figure 2.7 we see the arrangement of resistors in the termination region. In figure 2.8 it is shown in which way the performance of the current termionation improves with the number of distributed resistors and teeth respectively. The reflection coefficient increases when the number of teeth and resistors is increased. Still the overall performance does not remarkably improve anymore, when a certain number of teeth is exceeded. This depends on the dimensions of the cell. In this case of a 3 m wide center conductor the reflection coefficient improves only by about 3 dB for a change from 9 to 21 teeth. It should be noted that the determination of the distributed resistive values needs an increasing amount of computing power with an increasing number of teeth.

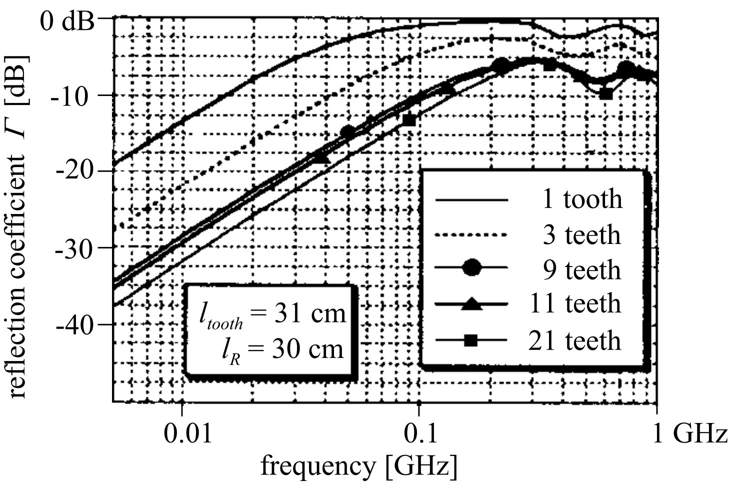

Figure 2.8: *The return loss vs. the frequency with different numbers of parallel teeth and resistors. No RF absorbers are present in the cell.* l_{teeth} *denotes the length of a tooth and* l_R *denotes the length of a resistor.*

2.4.2 Field termination

RF absorbers for EMC applications consist of relatively lossy material, e.g. of carbon loaded polyurethane foam, in order to absorb the energy of an incident wave. Usually they are pyramidal shaped (see figure 2.9).

The tapered geometry is chosen because of its good low-reflection properties as for the following aspects [15]: (a) Due to the sharp tip pointing towards

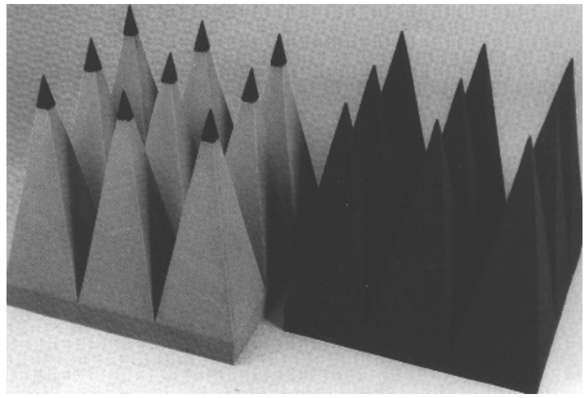

Figure 2.9: *The typical shape of broadband pyramidal absorbers.*

the incoming wavefront the change of the impedance is quasi-continuous. (b) The impedance is changing gradually as the wave propagates into the absorber assembly, as the area of the cross section that is filled with absorbing material is increasing continuously. (c) Specular reflections from the surface of the absorbers will be directed further into the absorbing structure rather than back into the environment.

The height of the absorber pyramids determines the lower frequency limit down to which the absorbers have a good return loss. As a rule of thumb the absorbers can be used down to a frequency where the height of the absorbers is half the wavelength. So for a height of 60 cm the lower frequency limit would be around 250 MHz. This limit will be one of the criteria for the choice of the RF absorbers.

In the GTEM cell the RF absorbers are arranged on a spherical surface on the rear wall of the cell. Due to the spherical arrangement the impedance is equal for the entire wavefront of the spherical wave and thus reflections are furthermore reduced.

3 Construction

3.1 Specifications

The aim of this work is the construction of a GTEM cell which allows testing the EMC properties of small electronic equipment with at least a size of a cellular phone in a frequency range from 30 MHz up to at least 1 GHz according to international standards for EMC measurements.

In IEC 1000-4-3 [5] a field uniformity of ± 3 dB in postion is required within a plane perpendicular to the incoming wave just in front of the position of the EUT. The 1/r behaviour of the field strength as a function of distance is not specified. The field unoformity of ± 3 dB in position should be achieved inside the whole testing volume of the GTEM cell. It will be shown that in the plane perpendicular to the incident wave a deviation of the field strength of about ± 1.5 dB can be expected inside the testing volume. The 1/r behaviour of the field in the longitudinal direction leads to a deviation of about ± 0.6 dB for a reasonable length of the testing volume of about 18 cm. The third factor taken into account is the standing wave ratio due to the termination region. To achieve a standing wave ratio of about ± 0.9 dB $= 1.23$ the return loss of the termination region must be better than $\frac{1.23-1}{1.23+1} = 0.1 = 20$ dB. The sum of all deviations is then ± 3 dB.

The field strength inside the testing volume as a function of frequency should not vary more than ± 3 dB from dc up to at least 1 GHz. The deviations should be recorded when calibrating the cell so that later measurement results can be corrected.

The termination of the cell should be constructed for an input power, that leads to a nominal field strength inside the testing volume of at least 10 V/m.

3.1.1 Dimensions

As the cell that was built in this work will be used not only for research but also for demonstration purposes for example within lectures one of the main specifications for the cell is the portability. This requirement restricts the overall dimensions and weight of the cell in order to ensure a certain portability and therefore leads to a relatively small cell when compared to the commercial ones. The size of GTEM cells that are usually used for industrial EMC testing can exceed a lenght of 9 m and fit test objects with a volume of over 1 m^3.

The overall length of this cell does not exceed 2.2 m and the weight is less than 50 kg. The dimensions of the GTEM cell, which is built in this work, is shown in figures 3.1 and 3.2.

The outer conductor is made of 2 mm aluminum sheets with extra bars for mechanical stability. A door of the size 30 cm x 25 cm is inserted into the sidewall. It is shielded to prevent leakage or interference from external fields.

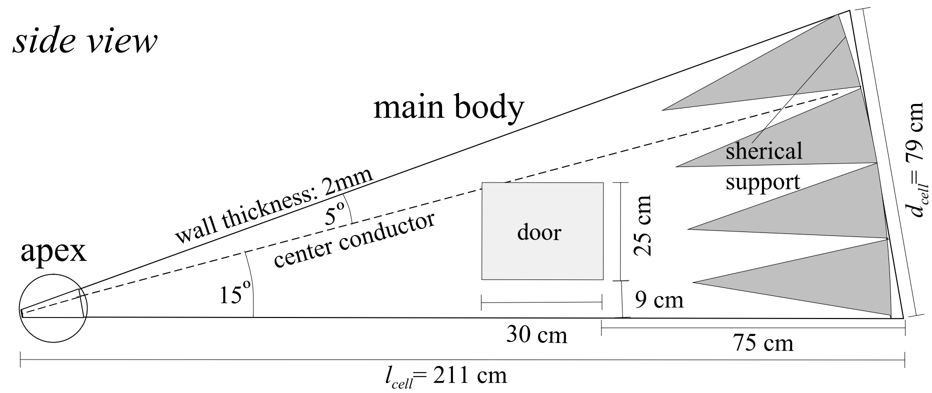

Figure 3.1: *The side view of the constructed GTEM cell. The apex is the detachable input section. The small size of the cell ensures its portability.*

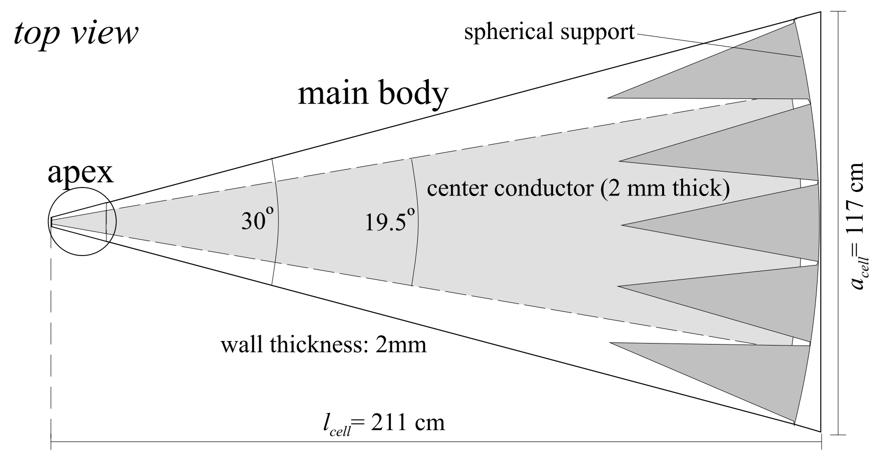

Figure 3.2: *The top view of the constructed GTEM cell. Its overall weigth is about 50 kg to which the RF absorbers contribute about a third.*

The center conductor is made of a 2 mm aluminum sheet and fixed to its position by nylon rods connecting it to the upper outer conductor. The rods have a diameter of 12 mm and are placed every 20 cm in pairs or triplets respectively.

The rear part of the cell consists of a rigid frame and an aluminum sheet. The sheet is bent into a spherical shape to support the spherical arrangement of the RF absorbers. The absorbers as well as the current termination assembly are attached to the rear wall before mounting the whole rear part to the cell.

To connect the current termination assembly to the center conductor a 2 cm overlap is left. The door is used to give access for the mounting. About 20 metal screws are holding the overlap together ensuring a good conduction. The effect of the overlap and the termination section on the characteristic impedance along the cell will be evaluated in chapter 3.5.

3.1.2 Testing volume

The testing volume is located in the center of the volume below the center conductor just in front of the tips of the RF absorbers. In this case the distance to the rear wall is 61 cm. (The absorbers are described in section 3.4.) At that position the distance from the center conductor to the bottom outer conductor is about 39 cm and the cell width is about 78 cm.

The vertical extension of the testing volume is restricted to $\frac{1}{3}$ of the distance h from bottom outer to center conductor. This is for two reasons: (a) The EM field strength is according to the above mentioned requirement constant enough only in that region and (b) larger equipment would itself alter the field strength too much as to allow reliable measurements.

To get a reasonable height of the testing volume an appropiate length is chosen. The typical dimension of the testing volume is shown in figure 3.3)

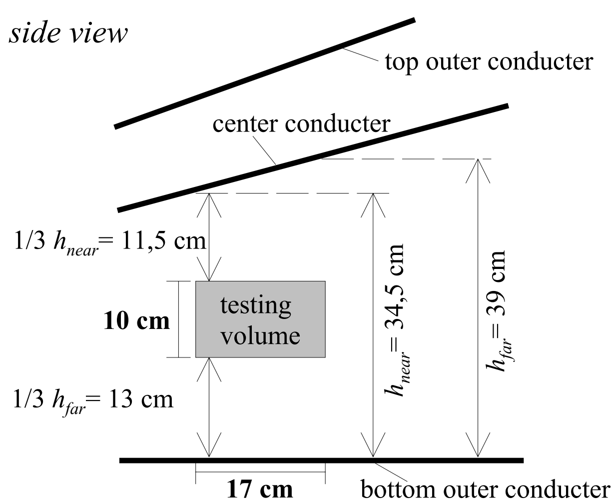

Figure 3.3: *The height of the testing volume is limited to about $\frac{1}{3}h$.*

The third extension, the width of the testing volume is usually likewise limited to a third of the width of the cell which is in this case about $a_{near} = 70$ cm. So the overall size of the electrical equipment that can be tested with the cell is not larger than 23 cm x 17 cm x 10 cm (width by length by height).

3.2 The apex

The apex is the transition from the 50 Ω coaxial cable to the rectangular transmission line. It is in this case made of brass and takes up about 10 % of the overall length of the cell. The front panel of it is made as small as possible and still large enough to mount a usual 50 Ω N connector.

The cross-sectional dimension at the beginning of the apex are $d_1 = 13$ mm by $a_1 = 19.5$ mm. (see figures 3.4 and 3.5 for all dimensions). The thickness u of the center conductor related to the height d_1 of the apex is about $\frac{u}{d_1} = 0.18$ and can therefore not be neglected when determining the width of the center conductor at the connection to the center pin of the connector. With help of the software QuickField (see chapter 2) a width of $w_1 = \frac{0.56}{a_1} = 11$ mm of the center conductor at the connection to the center pin of the connector was determined in order to achieve a characteristic impedance of 50 Ω.

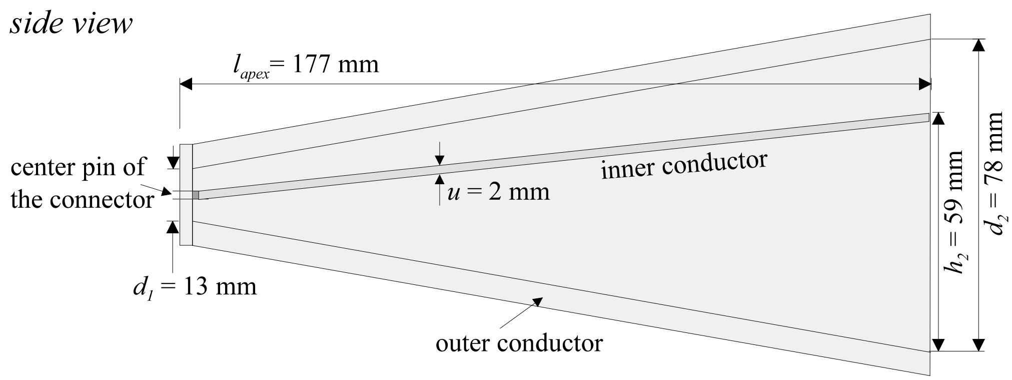

Figure 3.4: *Within the apex the relative vertical position of the center conductor h is changing from a ratio $h : d$ of* $1 : 2$ *to* $3 : 4$.

At the connection of the apex and the main body of the cell the width ratio between center and outer conductor has to be $\frac{w_2}{a_2} = 0.64$. The exact width of the center conductor could be determined for several points along the whole apex but a linear interpolation with the two given values is good enough in this case as will be shown in section 3.5. Therefore the width of the center conductor in the apex is increasing linearly along the length of the apex. There the center conductor is finally at the correct vertical position $h_2 = \frac{3}{4}a_2$.

To avoid reflections due to the abrupt change in diameter at the point where the center pin of the N connector is soldered to the center conductor the transition must be done very smoothly. Therefore on a length of about 1 cm the center conductor has a tapered shape (see figure 3.5).

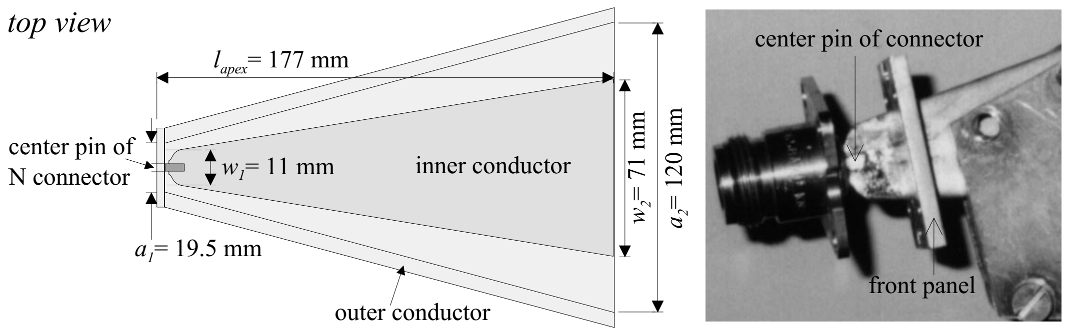

Figure 3.5: *The dimensions of the apex (l.) and a picture of the actual apex (r.). The soldered connection between the center pin of the connector and the center conductor is shown. The tapering of the center conductor reduces reflections that arise from the sudden change in the cross-sectional geometry.*

The apex is mounted on the main cell by means of flanges (see figure 3.6). This ensures high rigidity and good electrical connection between the apex and the main part of the cell. The center conductor has a constant thickness of 2 mm except at the connection of the apex and the main body of the cell. Here on a 1 cm long overlap section the two inner plates are held together with five M2.5 metal screws.

The effect of the tapered part and of the overlap section on the characteristic impedance is examined in chapter 3.5.

3.3 Resistive load section

In chapter 2 two concepts for the current termination were described which lead to a low reflection coefficient at frequencies up to at least 200 MHz.

For this relatively small cell the approach using tapered teeth is chosen for its easy realization when opposed to a large network of resistors. Accordingly to the patent of the GTEM cell [9] the number of teeth is fixed to three.

For designing the termination region the vertical distributed charge density in the center conductor must be known to adapt the width of each tooth to the current distribution in the center conductor. In this way the same current flows through each of the teeth which are then terminated by a 150 Ω resistor respectively.

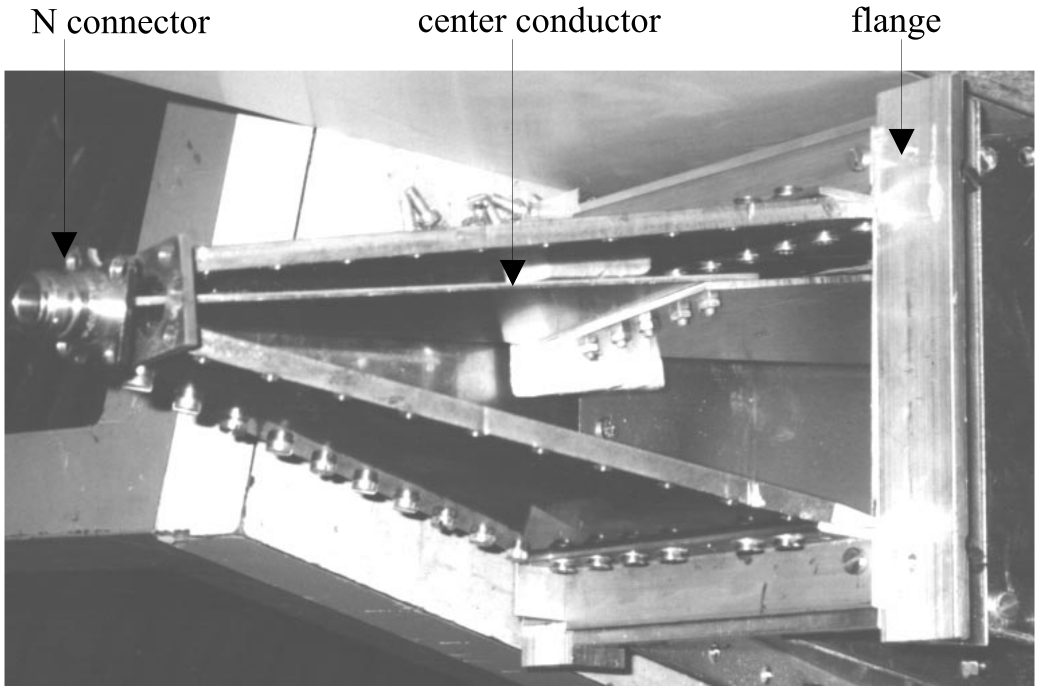

Figure 3.6: *The actual apex of the cell built in this work. It is mounted to the main body of the cell by flanges. One side of the outer conductor can be removed to give access to the screws at the overlap region. The connector is attached to the center conductor before it is mounted to the front panel of the apex.*

To find the current distribution in the center conductor the field distribution at its surface is examined with help of the the finite element method software Quickfield that was mentioned in section 2.3. After having found the field distribution one can directly derive the charge distribution on the surface of the conductor which is proportional to the current distribution in the center conductor.

The results in figures 3.7 and 3.8 are obtained from Quickfield. For the calculations the potential of the center conductor is fixed to 1 V and the distance between the center conductor and the bottom outer conductor is $h = 1$ m. This leads to a nominal electric field strength in the testing volume of $E_{nom} = 1$ V/m. This value is found approximately in the center of the volume below the center conductor. It is taken as a reference value to which all the results from the calculations made with Quickfield are related (if not defined differently).

The maximum of the field strength is found at the edges of the center conductor as shown in figure 3.7. However the absolute value of the field strength at the edges can be obtained from the approximations only roughly, because the

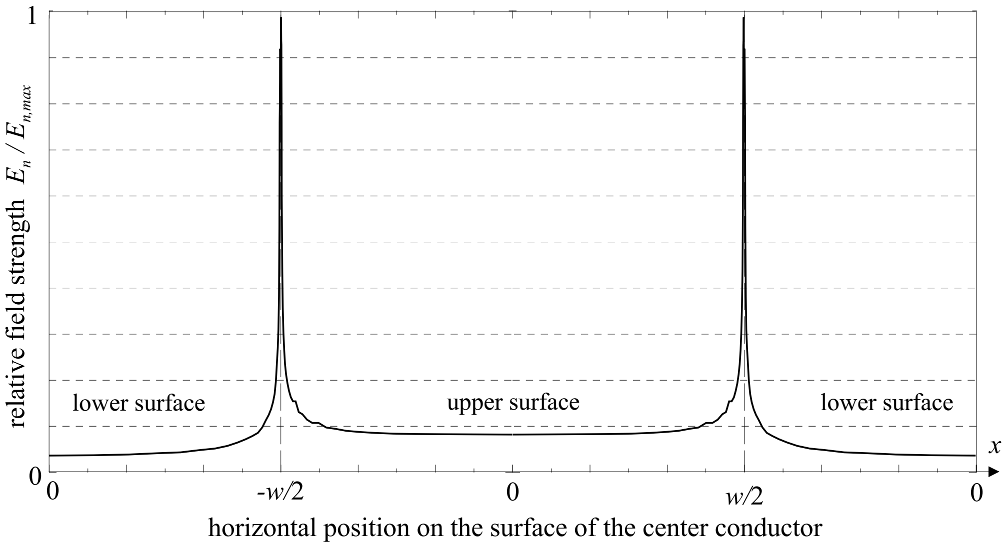

Figure 3.7: *The field strength along the surface of the inner conductor related to the maximum field strength at its edges The x axis is wrapped around the edges, thus the* 0 *on the left denotes the same location as the* 0 *on the right which is the center of the lower surface. Whereas the* 0 *in the center denotes the center of the upper surface of the center conductor.*

numerical approach is not accurate enough to either calculate the steep slope of the field strength towards the edges of the center conductor nor therefore the maximum value of the peaks.

In figure 3.8 the absolute values for the region around the middle of the center conductor are shown. The relative field strength in the center of the upper surface is 3 times higher than the reference value in the center of the volume below the center conductor as the distance to the upper outer conducter is $\frac{1}{3}$ of the distance h to the botton one. The relative field strength in the center of the lower surface is about 1.3 times as high as the reference value.

With help of Quickfield three parts of the center conductor are determined that carry an equal charge. Hereby the initial width of the three teeth can be determined. The center tooth is wider than the two lateral ones as the charge density is higher towards the edges. The width ratio of center tooth to lateral teeth can be determined: In order to achieve an equal charge (and therefore an equal current) on each of the teeth the ratio between the width of the middle tooth and the lateral ones is 1.65.

The width of the center conductor is 51 cm near the tips of the absorbers which is 61 cm from the rear wall. So the initial width is 51 cm$\cdot\frac{1.65}{3.65} = 23$ cm for the center tooth and 51 cm$\cdot\frac{1}{3.65} = 14$ cm for the lateral ones.

As was shown in chapter 2 the influence of the RF absorbers on the charac-

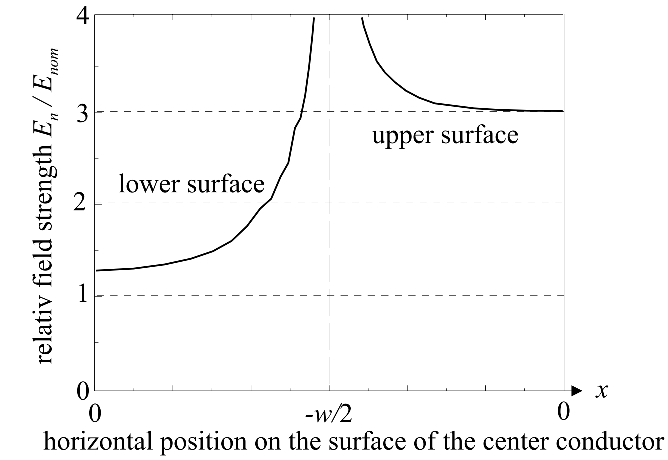

Figure 3.8: *The field strength along the surface of the center conductor. It is related to the field strength in the center of the volume below the center conductor.*

teristic impedance of the line could be exactly determined. In this work an approach is chosen that does not model the effect of absorbers, as the complex conductivity is not known for all frequencies.

For determining the shape of the teeth one tooth was considered and afterwards split into three teeth with the above calculated width ratio of 1.65. One variable is the final width of the teeth towards the rear wall where the RF absorbers fill the cross section completely. If the permittivity of the material is known, the final width could be determined. However, the correct value might depend on the frequency and can therefore only be optimised as for a minimal deviation e.g. at $0 - 300$ MHz.

During the design of the teeth the permittivity of the absorbing material, that is given for 2 frequencies in section 3.4, was still unknown. So the width at the end of the center tooth and the lateral teeth was chosen to 2.5 mm and 1.5 mm respectively. Those values result in a characteristic impedance of 330 Ω close to the rear wall when there are no RF absorbers present in the cell.

After having determined the initial and final width an approach is neccessary that changes the characteristic impedance of the cell smoothly towards the rear wall. The concept of a tapered transition for transmission lines was applied to this problem.

From [16] we find a method for an exponential tapering. This means the characteristic impedance of the line varies exponetially in the longitudinal direction like

$$Z = e^{(z/l) \ln Z_L} \tag{3.1}$$

where l denotes the length of the transition and Z_L the final characteristic impedance which is in this case $Z_L = 330\ \Omega$. z denotes the longitudinal position.

To determine the shape of the teeth still no straight forward method is usable, as there is no closed formula relating the width of the center conductor and the impedance of the transmission line. It was done by choosing $i = 12$ values for the width of one tapered tooth starting from the width $w = 51$ cm at the position of the tips of the absorbers going down to $w_{12} = 0.7$ cm at the rear wall. Then the impedances Z_i that correspond to each width w_i were calculated by using the software Mathematica and the numerical method described in chapter 2.3. Afterwards (3.1) is solved for z to determine the longitudinal position z_i that is related to the width w_i

$$z_i = l_{tooth} \cdot \frac{\ln Z_i}{\ln Z_L} \tag{3.2}$$

The values for the width have to be adapted to the increasing cross-sectional area of the transmission line. The width as a function of z is then found by linear interpolation between the 12 positions z_i. Afterwards the width of the three teeth is determined considering the width ratio of 1.65. Finally the shape of e.g. the center tooth in figure 3.9 is found, where $v_i = w_i \cdot \frac{1.65}{3.65}$.

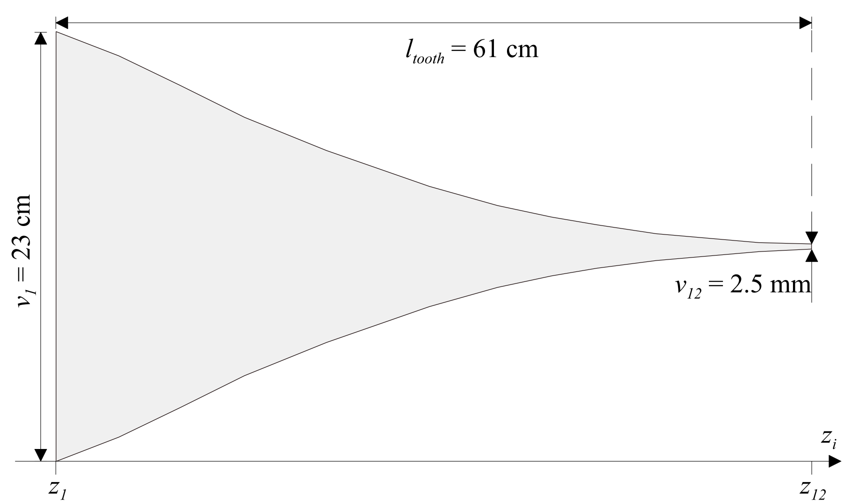

Figure 3.9: *The shape of the center tooth for the current termination to make an exponential tapering from 50 Ω to 330 Ω and furthermore taking the opening angle of the transmission line into account.*

Printing the shape on circuit boards is an easy way to obtain the three teeth. Furthermore the necessary three 150 Ω resistors can easily be soldered onto the board at the end of the teeth. The boards are then mounted to the back wall. To achieve an exact 150 Ω load per tooth three parallel carbon film resistors were chosen, i.e. with the values 392 Ω, 464 Ω and 511 Ω. Each of the resistors has a nominal maximum power consumption of 400 mW, i.e. a total maximum power consumption of about $P_{max} = 3$ W. According to (2.2) with an input power of 3 W in susceptibility tests a nominal field strength of $E_{max} = 33$ V/m can be obtained within the testing volume. This value will be sufficient for the use of this cell in research purposes.

The termination assembly is mounted to the back wall in a manner that it is still possible to disassemble it and replace it by another construction, if it is needed for improving the properties of the cell.

3.4 RF absorbers

The RF absorbers terminate the waves at a frequency range starting from a frequency that depends mainly on the length of the pyramids. As a rule of thumb the height of the absorber pyramids should be larger than half the wavelength. So for a height of 60 cm the lower frequency limit would be around 250 MHz.

They are assembled to the rear wall on a spherical surface to affect one complete wavefront as homogeneously as possible. A wide enough gap of 2 - 3 cm must be left for the resistive termination assembly because the RF absorbers have a larger influence on the characteristic impedance the closer they are situated to the center conducter.

In the following three different RF absobers are compared that were available at the time this cell was designed:

The *Rantec* FerroSorb 300 has an overall height of 30 cm and consists of a ferrite tile layer bonded to polyurethane foam absorbers which are a section of a pyramidic structure, i.e. the tips were skipped. In the frequency range from 30 MHz to 1 GHz the absolute reflection coefficient is better than -20 dB and in $1 - 5$ GHz it is better than -12 dB (see figure 3.10).

The German company *Ecomp* offers the Broadband Pyramidical Absorber EPP 52 with an overall height of 50 cm. Measurement results were available only for frequencies above 500 MHz and here it shows a reflection coefficient better than -30 dB (see figure 3.11).

The dimensions of the *Rantec* broadband absorber EMC-24CL are overall height of 61 cm a base height of 15.2 cm and the height of the pyramids 45.7 cm. Its reflection coefficient is better than -20 dB for frequencies above 200 MHz and -13 dB at 100 MHz (see figure 3.12). The (complex) permittivity

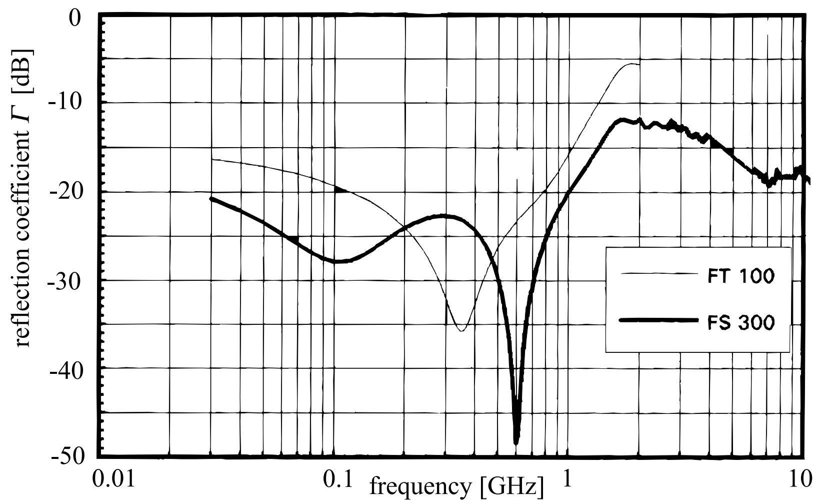

Figure 3.10: *The absolute value of the reflection coefficient of the Rantec FerroSorb 300 RF absorbers. FT 100 denotes the ferrite tile alone.*

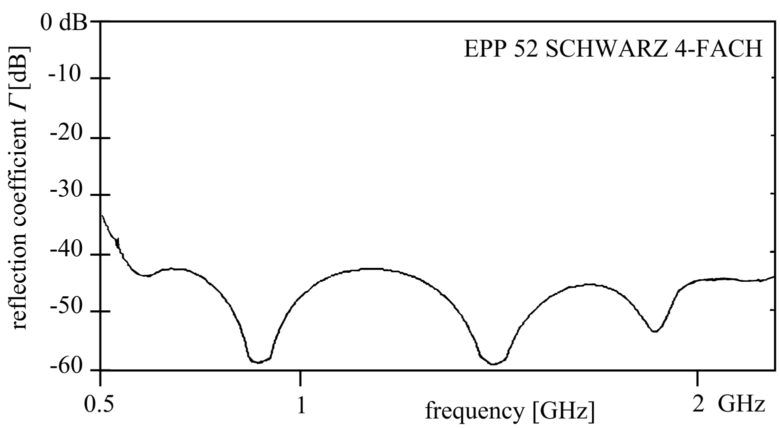

Figure 3.11: *The absolute value of the reflection coefficient of the Ecomp EPP52 RF absorbers.*

was given as $\epsilon'(30\ \text{MHz}) = 7$, $\epsilon'(1\ \text{GHz}) = 1$ and $\epsilon''(30\ \text{MHz}) = 12$, and $\epsilon''(30\ \text{MHz}) = 4$.

The FerroSorb 300 has good absorption properties at lower frequencies but it shows a relatively bad performance at frequencies above 800 MHz. The EPP 52 absorbers of the company Ecomp could not be rated as the reflection values for low frequencies were not available. So the EMC-24CL absobers mentioned last seem to be the best suitable for a broadband application especially with regard to the relatively good low frequency absorption.

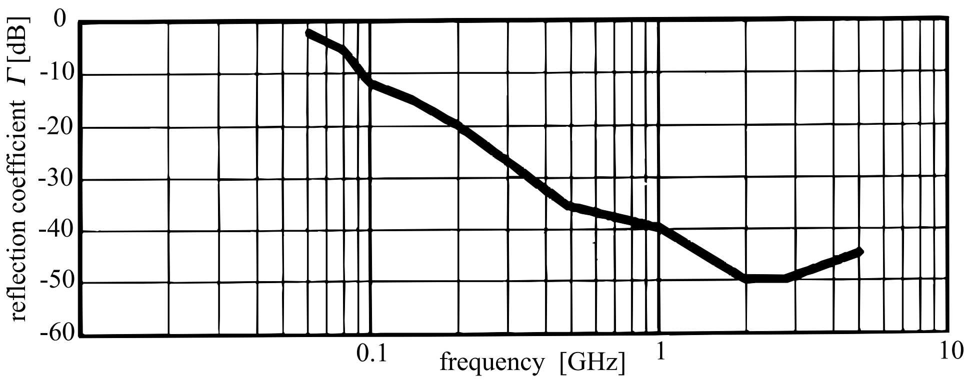

Figure 3.12: *The absolute value of the reflection coefficient of the Rantec EMC-24CL microwave absorbers at normal incidence.*

3.5 Evaluation of the design

For evaluating the design of the cell different measurements were made:

(a) time domain reflectrometry (TDR) measurements were performed in order to verify a constant characteristic impedance $Z = 50\ \Omega$ along the transmission line. The TDR measurements were carried out with the HP 54120T Digitizing Oscilloscope and the 4 channel HP 54121 Test Set. The frequency range of the oscilloscope is 20 GHz. The effective TDR rise time is 45 ps.

(b) The reflection coefficient was measured with the HP 8530 Network Analyser System to examine the return loss up to a frequency of 5 GHz. According to the specifications the return loss should be 20 dB from 30 MHz to at least 1 GHz.

3.5.1 Transition in the apex

A region of special interest is the transition inside the apex from the coaxial connector to the rectangular transmission line. The apex was designed before the main body of the cell, thus measurements of the characteristic impedance and of the reflection coefficient were done with the open-ended apex.

In figure 3.13 two phases of the design of the transition from the coaxial connector to the rectangular transmission line are shown.

The transition section is illustrated before and after the rounding of the center conductor. The tapering was improved until a minimum impedance level of 50 Ω was reached. (For the transition region see as well figure 3.5.) Inside the N connector and therefore fixed the characteristic impedance has a peak of 55 Ω.

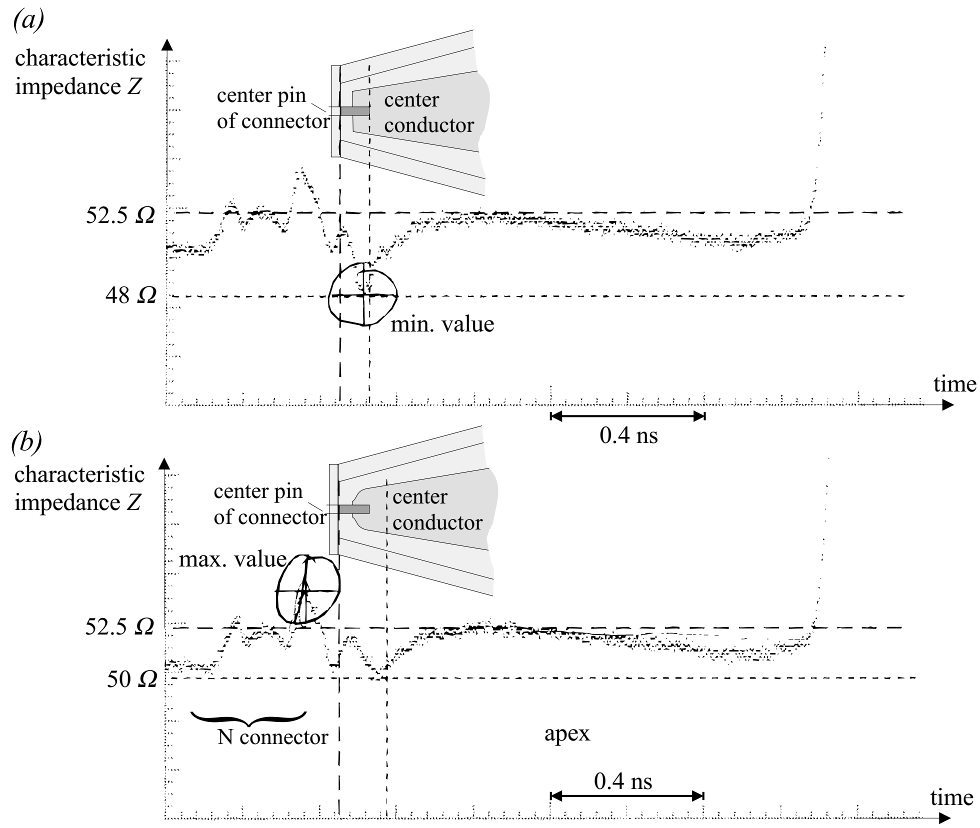

Figure 3.13: *TDR measurements that show two phases in the design of the transition inside the apex which is illustrated. (a) The impedance drops down to* 48 Ω *due to the sharp corners of the center conductor (see ⊕). (b) After having rounded the corners the impedance does not drop below* 50 Ω. *The* 55 Ω *peak (see ⊕) is inside the connector.*

The characteristic impedance is plotted against the return time of a step. An interval of 0.4 ns on the coordinate-axis corresponds to a distance of 6 cm.

To evaluate the frequency response the reflection coefficient of the apex was compared to that of a 20 cm long 50 Ω coaxial cable. For those measurements time gating was used, which simulates a matched load at the open end of the apex and of the reference cable respectively (see figure 3.14 (a)).

Below 2 GHz the reflection coefficient of the apex is below −30 dB. The results below 500 MHz are not so reliable as the reflection coefficient of the reference cable is too low when compared to the results for the cable with a matched broadband load that was measured without time gating (see figure 3.14 (b)).

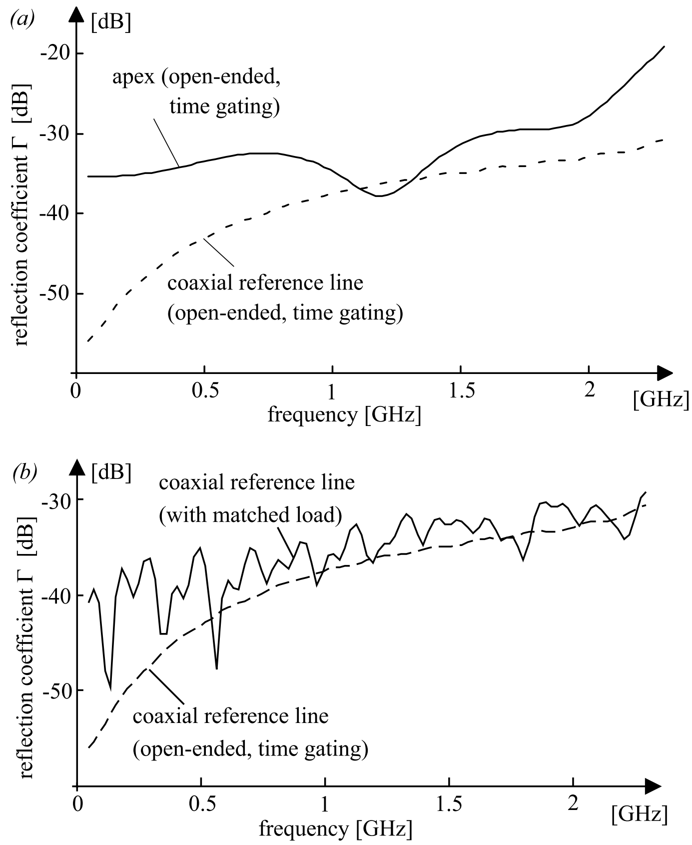

Figure 3.14: (*a*) *The reflection coefficient of the apex compared to a coaxial cable of the same length. Time gating simulates a matched load.* (*b*) *The frequency response of the open-ended coaxial cable compared to the response of the cable with a matched load and without time gating.*

3.5.2 Overlap section in the apex

After assembling the main body of the cell and adjusting the vertical position of the center conductor the overlap section of the center conducter between apex and main body is examined. In figure 3.15 the strongest step within the characteristic impedance Z is from to 48.75 Ω at t_0 and up to 51.75 Ω within 0.1 ns. A similar step in figure 3.13 leads to an acceptable reflection coefficient below -20 dB (see figure 3.13) up to 2.5 GHz above which the cell is not going to be used.

It should be noted, that in the assembled cell the center conductor is in one piece and therefore the center pin of the N connector might easily be slightly displaced and deformed during the mounting procedure of the rear wall.

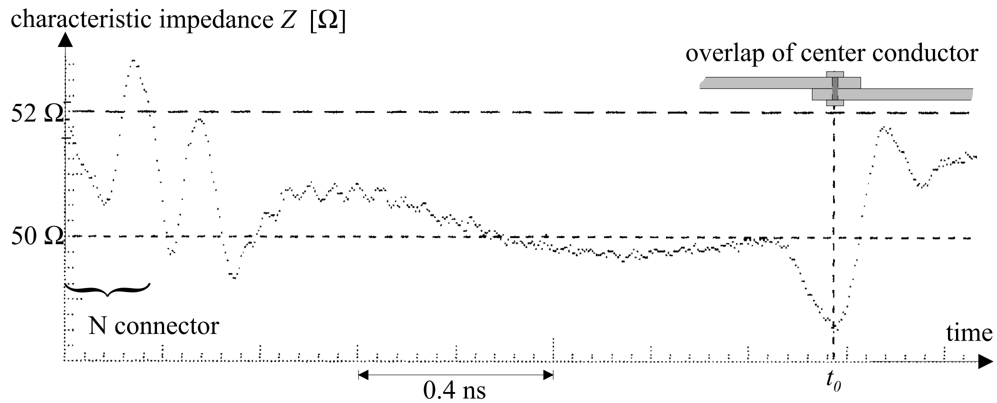

Figure 3.15: *The characteristic impedance along the apex after having mounted it to the main body of the cell. The overlap of the center conductor is illustrated.*

3.5.3 Position of the center conductor

After the center conductor has been fixed to its optimal vertical position the characteristic impedance has a constant level of about 50 Ω.

In figure 3.16 the influence of the nylon rods is illustrated. The rods were placed every 20 cm. At the position of each pair or triplet of rods the charateristic impedance drops by $1-3$ Ω. The influence decreases with the increasing cross-sectional area towards the rear end. To decrease reflections due to the rods (a) the two rods closest to the flange were replaced with 8 mm rods and (b) from each the pairs and triplets one rod was removed. This does not impair the rigidity of the center conductor.

In figure 3.17 the final results are shown. After replacing the first two rods with thinner ones the drop in the impedance is only half as large but still larger than that of the other rods. Along the remaining part of the cell the drop in the characteristic impedance due to the nylon rods is smaller than the effects inside the apex, which lead to an acceptable reflection coefficient.

Another drop is observed at the overlap section, where the 3 teeth for the current termination are connected to the center conductor by means of several M4 metal screws.

3.5.4 Termination section

After the vertical position of the center conductor has been adjusted and the rear wall with the attached termination section installed the characteristic impedance in that section was evaluated.

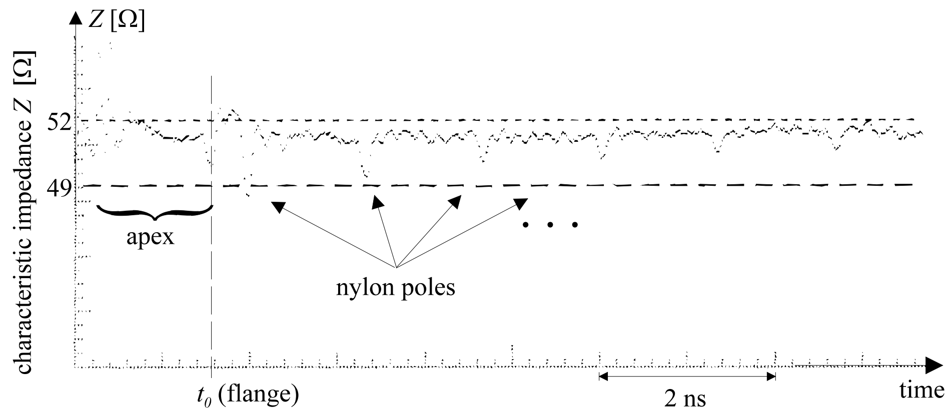

Figure 3.16: *Before modifying the construction the characteristic impedance drops by* $1 - 3\ \Omega$ *every* 20 *cm due to the nylon rods.*

In the termination section the characteristic impedance drops down to 40 Ω (see figure 3.18). This is due to a underestimated influence of the RF absorbers. i.e. the tapering of the teeth is not appropiate. It will be shown in the following section that due to this the specification for the lower frequency limit is not met. However, for frequencies below 20 MHz the 50 Ω resistance is again a matched load.

To improve the performance of the termination section a second set of teeth could be designed. From figure 3.18 can be stated that the teeth taper too little towards the rear wall. A narrower tapering around the center of the teeth will raise the characteristic impedance towards 50 Ω and therefore lower the reflections at lower frequencies.

A similar structure has been examined in [17]. In that case a similar drop in the characteristic impedance down to less than 40 Ω has been modelled and the VSWR numerically calculated. The result was a maximum reflection coefficient of −15 dB at about 50 MHz. Similar values are found for this cell in the following sections.

3.5.5 Reflection coefficient

In figure 3.19 *a*) the reflection coefficient of the cell up to 1 GHz is shown. At 40 MHz the reflection coefficient reaches a maximum of −16 dB. This is due to the unsufficiently exact design of the current termination section, i.e. the tapering of the teeth. The problems and limits of this design were discussed in section 3.3. Improvements were discussed in the previous section. In this work no changes were made to the termination section, as only a small frequency range is affected by the mismatch.

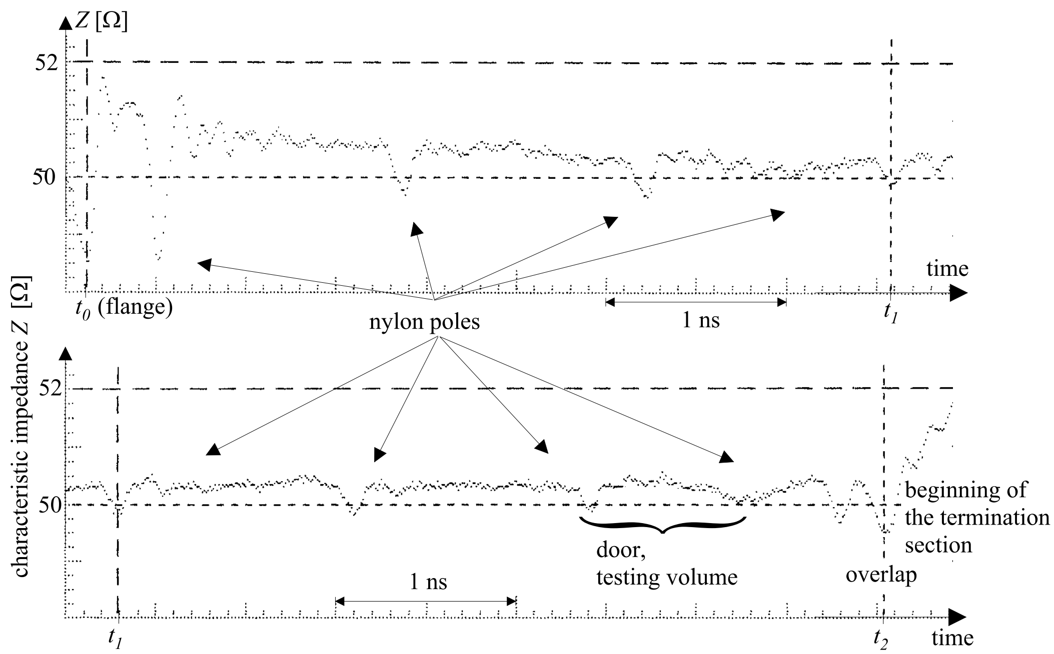

Figure 3.17: *After removing every second nylon rod the characteristic impedance drops only by 1 Ω at the position of the rods. The first pair of rods has not been changed. Another drop occurs at the overlap, where the teeth for the current termination are connected to the center conductor (t_2).*

In figure 3.19 *b*) the reflection coefficient of the cell up to 5 GHz is shown. Peaks appear at integer multiples of 750 MHz. At this frequency $\lambda/2 = 20\ cm$. A reason is the placement of the nylon rods at every 20 cm. Although each of the rods has a small influence, this periodic structure gives rise to resonances at the integer multiples of 750 MHz.

After removing half of the nylon rods the effect was decreased. The concept of fixing the vertical position of the center conductor by nylon rods is nevertheless very practicable as each of the rods alone does not affect the performance very much. The distance between the nylon rods though should be chosen differently for each successive pair so that the resonance effects do not occur at some common frequencies.

As a last alteration of the setup the whole center conductor has been moved 1 - 2 mm towards the apex to release the tension in the center pin of the connector. The center conductor had been slightly displaced during the mounting of the rear wall. This was observed in TDR measurements, when the characteristic impedance had changed in the tip of the apex. This problem was not approached in this work but could be solved by a stronger plastic support for

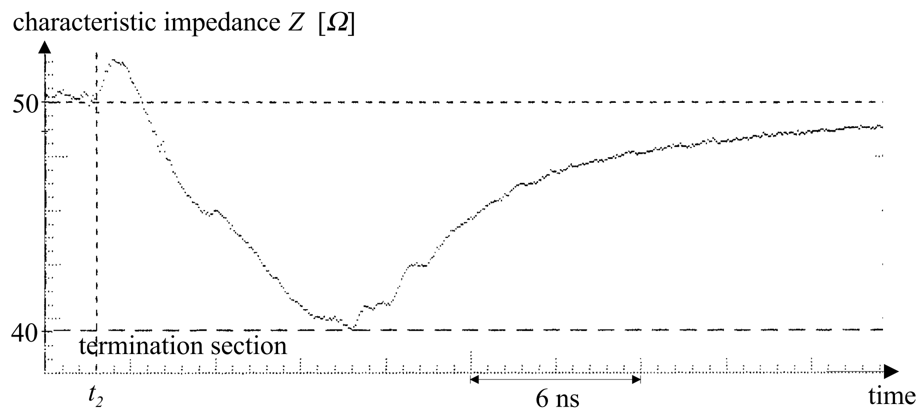

Figure 3.18: *In the termination section the characteristic impedance drops down to* 40 Ω, *which is due to the RF absorbers.*

the center conductor inside the apex. The additional plastic material will have an the effect on the characteristic impedance, which has to be compensated by reshaping the center conductor at the position of the plastic support.

The final setting is denoted by the solid line in figure 3.19. The reflection coefficient is below −16 dB between 20 − 80 MHz and below −20 dB up to 2.8 GHz, so the specifications are met at least for the higher frequencies.

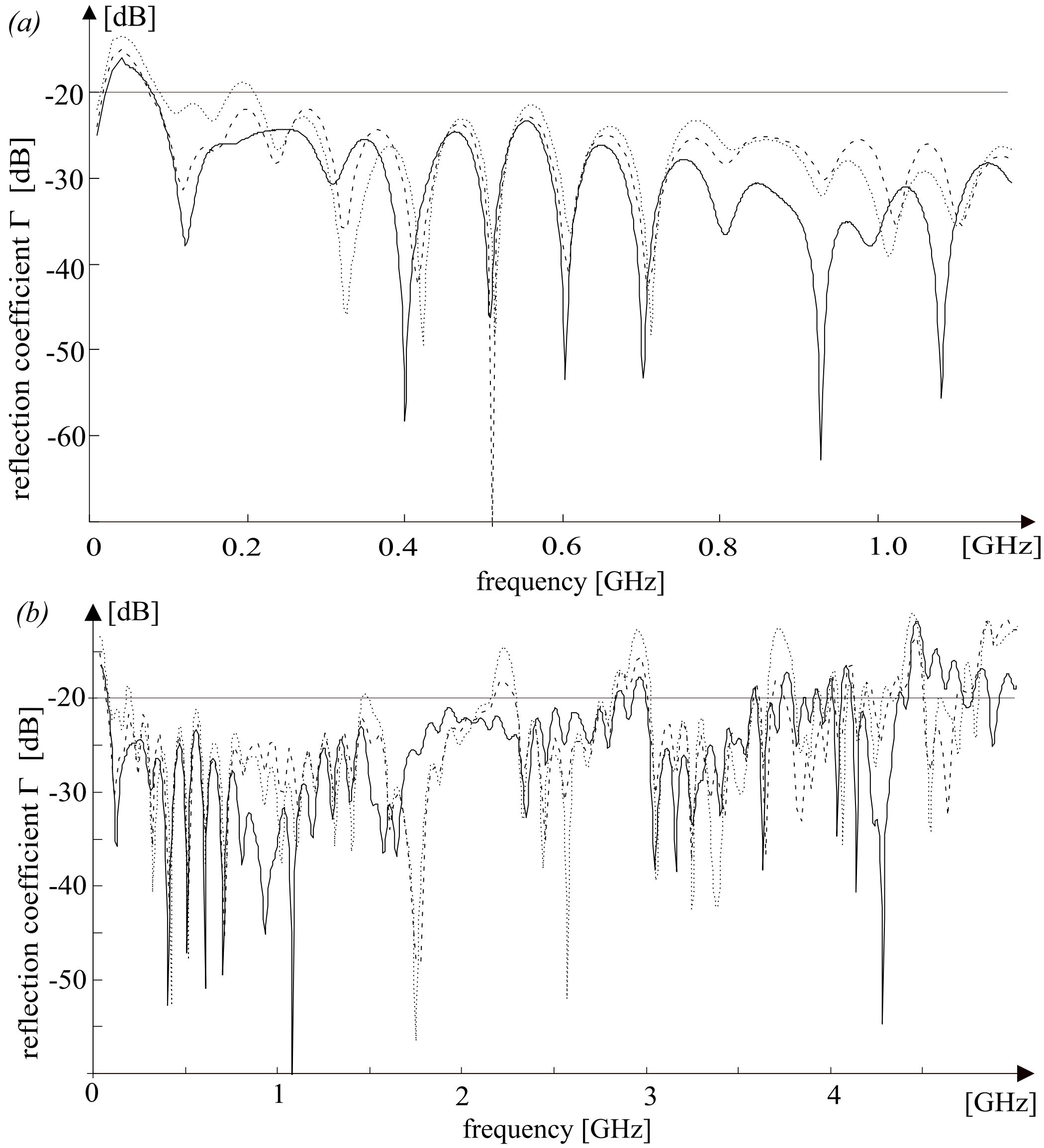

Figure 3.19: *The improvement of the performance of the cell during three stages of construction is illustrated with help of the reflection coefficient. From stage 1 ($\cdots$) to stage 2 ($---$) some of the nylon rods were removed. In the final stage (—) the center conductor has been moved $1-2$ mm towards the apex to release the tension in the center pin of the connector. Peaks appear at integer multiples of 750 MHz. At this frequency $\lambda/2 = 20$ cm which is the distance between the periodically assembled nylon rods.*

4 Measurements

Typical applications of the GTEM cell are radiated EMC tests of electronic equipment [21]. Those test include susceptibility tests, where the device is exposed to radiated disturbances, and measurements of radiated emissions of the device. Methods of the radiated EMC tests are described.

Results from calibration measurements are presented that verify the field uniformity in the testing volume of the GTEM cell built in this work. Results from antenna measurements are presented. They indicate a possiblility to use the GTEM cell for measurements of certain antenna properties.

4.1 Susceptibility measurements

For testing an electronic device for its susceptibility to continuous or pulse-type electromagnetic fields it is placed in the testing area and a signal generator is connected to the input of the cell (see figure 4.1). The performance of the EUT is then monitored as a function of input power.

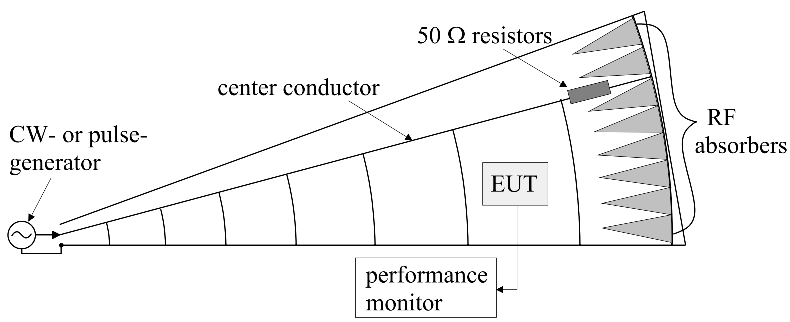

Figure 4.1: *In susceptibility tests the input is connected to a CW- or pulse-generator. The EUT is then exposed to a slightly spherical field.*

Due to the small opening angle of the cell the waves are only slightly spherical so the EUT can be considered to be exposed to a planar wave. This is an important aspect that makes the procedure standardised and the results obtained from a GTEM cell comparable with those from other standard measurements.

The current in the center conductor is terminated in a resistive load section with a total of 50 Ω, while matching the current distribution in the center conductor. The electromagnetic waves that are generated in the cell volume and applied to the EUT are terminated in the RF absorbers that are arranged at the rear wall on a spherical plane (see figure 4.1).

For measuring the electric field strength inside the cell the Holaday GRE-03 electric field probe combined with the broadband exposure meter Holaday HI-3002 has been used. The probe consists of three orthogonally assembled Schottky-diode detectors, so the total value of the field strength at each measuring point is determined. The detectors are placed inside a styrofoam ball of 10 cm diameter and considered to be situated in the center of the sphere.

The effects of the probe wires on the electric field are minimized by using high-resistive dc-cables. The equipment was calibrated at the Finnish Center For Radiation And Nuclear Safety (STUK) for several frequencies between 10 and 300 MHz. The accuracy of the calibration was given as ± 1 dB. Above 300 MHz no calibration measurements of the field uniformity were performed, as the necessary calibrated field probes or calibration facilities were not available.

To verify a constant input power at the port of the cell, the output power of the *Mini-Circuits* ZHL-2-8 amplifier was measured at $10 - 300$ MHz with the HP 8487A power sensor and the HP 437B power meter. The levels were then used to correct the results of the measurements. The return loss of the ampifier output is about -12 dB and the cell is well matched (see chapter 3). Therefore no resonances were observed, which could cause fluctuations in the input power after connecting the cell to the amplifier.

As shown in chapter 2 the field strengh in the cell is decreasing in a $1/r$ manner in the longitudinal direction. To verify the results shown in figure 2.3 the field strength was measured along the longitudinal direction of the cell. The field probe was moved along at the center of the cross-sectional area at $y = \frac{1}{2}h$. The measurements were done at 8 positions within a distance of $\zeta = 0 - 35$ cm from the tips of the absorbers (see figure 4.2).

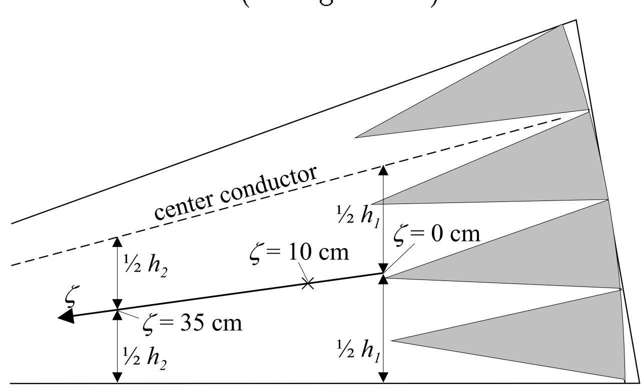

Figure 4.2: *The setup of the measurement of the field strength along the longitudinal axis in the volume below the center conductor.*

Measurements were performed at 10, 30, 60, 80, 100, 140, 180, 230, 275 and 300 MHz. The results are included in appendix A. The results were corrected for the $1/r$ behaviour of the field strength along the z-axis. This is done in such a way that the results relate to the center of the testing volume at $\zeta = 10$ cm, where $h|_{\zeta=10} = 37$ cm. The linear correction term is -1.85 dB at $\zeta = 35$ cm and $+0.65$ dB at $\zeta = 0$ cm.

In figure 4.3 a) and b) the field strength is plotted against ζ for several frequencies between $10 - 300$ MHz whereas in c) and d) the field strength is plotted against the frequency for different values of ζ.

As a function of position the field strength is within ± 0.7 dB for each frequency. This corresponds well to the expected $1/r$ behaviour. However, the field strength as a function of frequency shows deviations of up to ± 1 dB. The greatest deviations can be observed between 30 and 80 MHz. This might be due to the the fact, that at those frequencies the return loss of the termination section is not as good as for the other frequencies. The relatively high deviation at 180 MHz could not be explained.

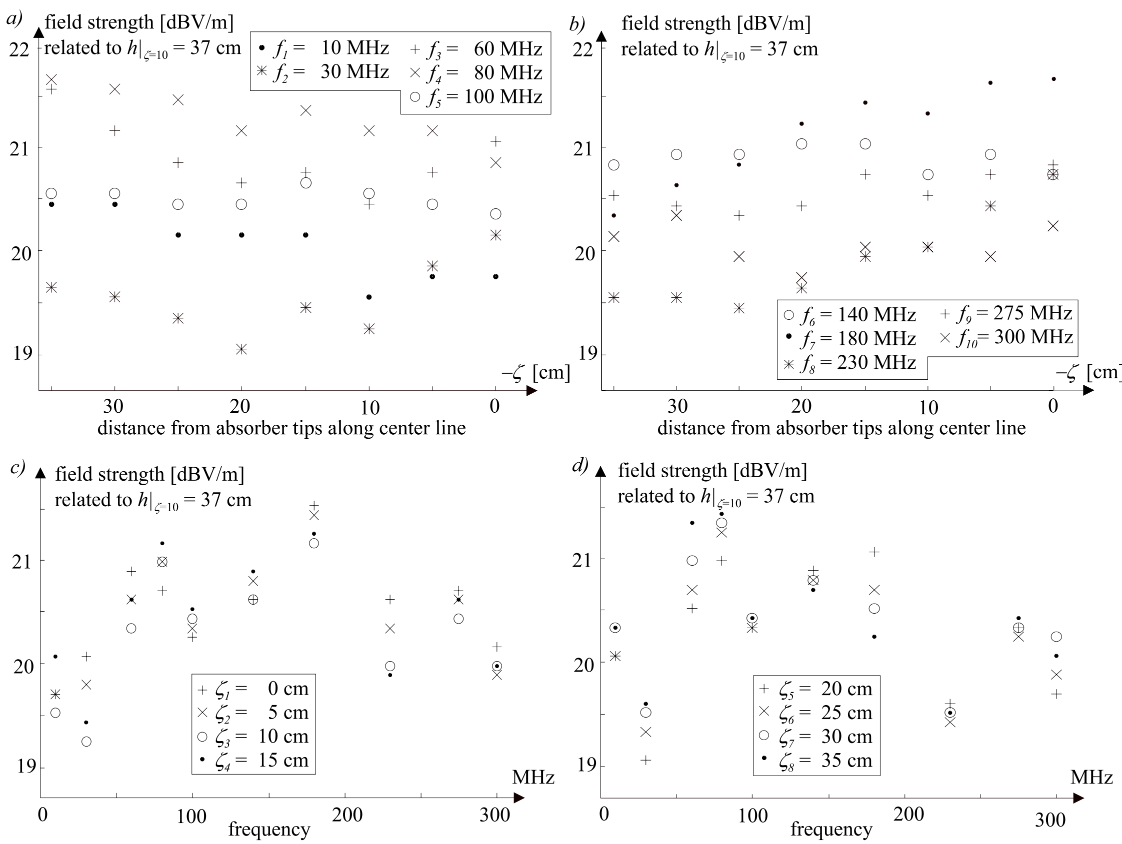

Figure 4.3: *The measured total field strength at $y = h/2$ as a function of longitudinal position and frequency. The field strength is corrected for its $1/r$ behaviour, so it refers to $\zeta = 10$ cm, i.e. to the center of the testing volume.*

In the measurements an input power of $P = 24.6$ dBm ($= 0.29$ W) was used. According to (2.2) this yields in a nominal field strength in the testing $E_{nom} = 10.3$ V/m ($= 20.3$ dBV/m) which corresponds well to the measured field strength at $\zeta = 10$ which varies from $19.2 - 21.3$ dBV/m.

The field strength was then measured at 33 positions within the testing volume. The numerical results are included in appendix A. In figure 4.4 the field distribution at 100 MHz is illustrated in 3 horizontal planes, i.e. the top, center and bottom planes of the testing volume (see figure 3.3). The results obtained with the input power of $P = 24.8$ dBm ($= 11.8$ dBV).

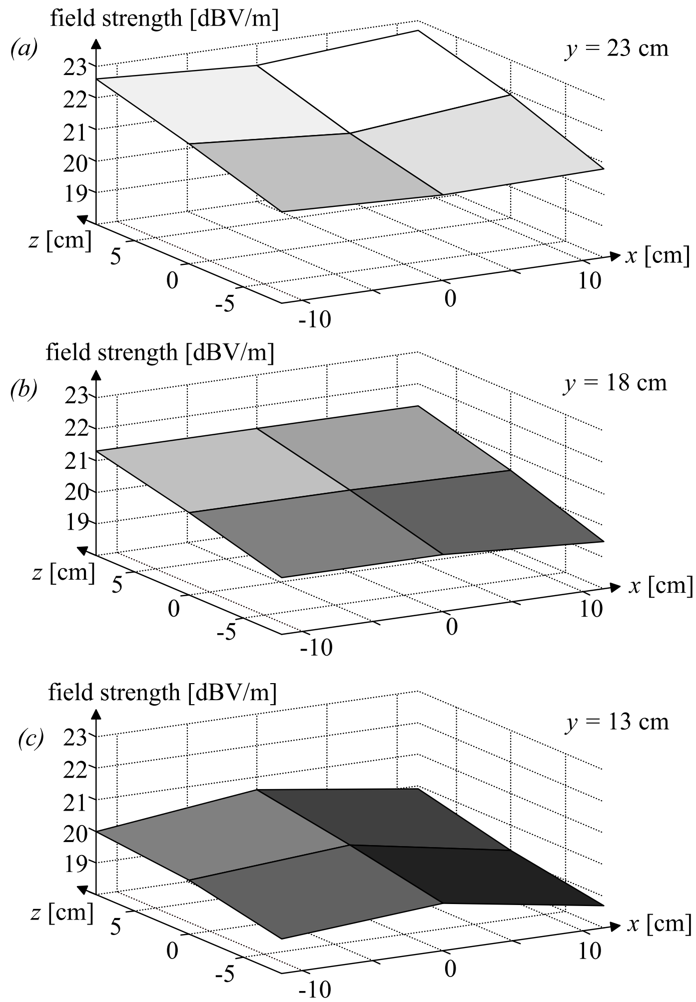

Figure 4.4: *The field strength pattern at* 100 *MHz at* $y = 13, 18$ *and* 23 *cm from the bottom outer conductor. The input power is* 24.8 *dBm.*

At 100 MHz the difference between the maximum value (22.7 dBV/m) and the minimum value (18.7 dBV/m) is 4 dB. This deviation of ± 2 dB is not exceeded for higher frequencies (up to 300 MHz). The deviations in one point as a function of frequency are smaller than ± 2.5 dB. It must be noted though that at frequencies below 100 MHz the deviation as a function of position is up to ± 3.5 dB (see appendix A).

In figures 4.5, 4.6, 4.7, 4.8 and 4.9 numerical results from a two-dimensional electrostatic field approximation for the TEM mode are illustrated. The pictures are made with help of the software Quickfield (see chapter 2).

In figure 4.5 the vertical field strength in the cross section at three different heights above the bottom outer conductor is shown. The field strength in the center of the testing volume ($y = \frac{1}{2}h$) is slightly below the nominal value. This is caused by the offset of the center conductor, due to which the field pattern is changing from a quite uniform one towards the pattern observed in a coaxial line. In figure 4.6 the equipotential line pattern in the cross section is shown.

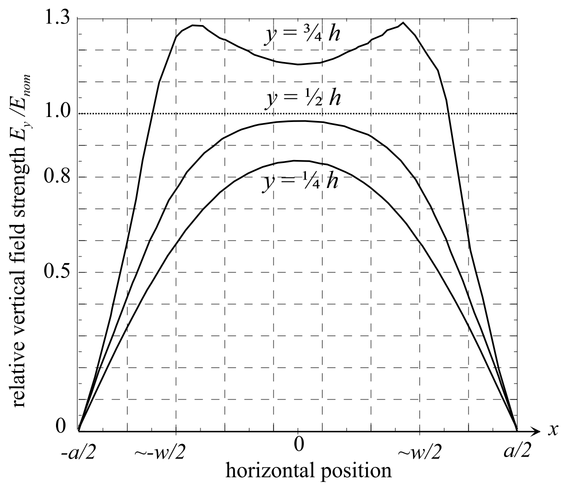

Figure 4.5: *The simulated field strength versus x at three different vertical positions y related to the nominal field strength in the testing volume.*

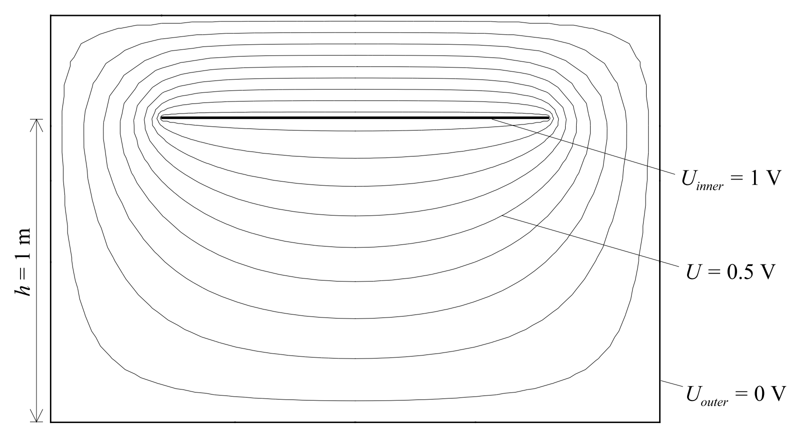

Figure 4.6: *Simulated equipotential lines in the cross section of the cell.*

In figures 4.7 and 4.8 the simulated vertical and horizontal electric field distributions within the cross section are illustrated. The simulated total field strength in the cross section is shown in figure 4.9. The values are related to a nominal field strength in the testing volume of $E_{nom} = 1$ dBV/m.

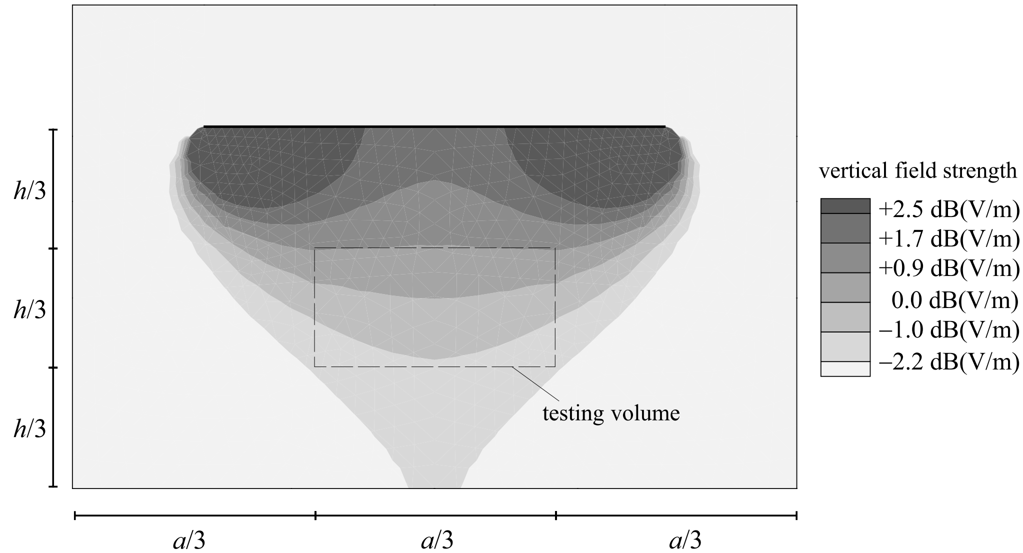

Figure 4.7: *The absolute value of the simulated vertical field strength in the cross section of the cell.*

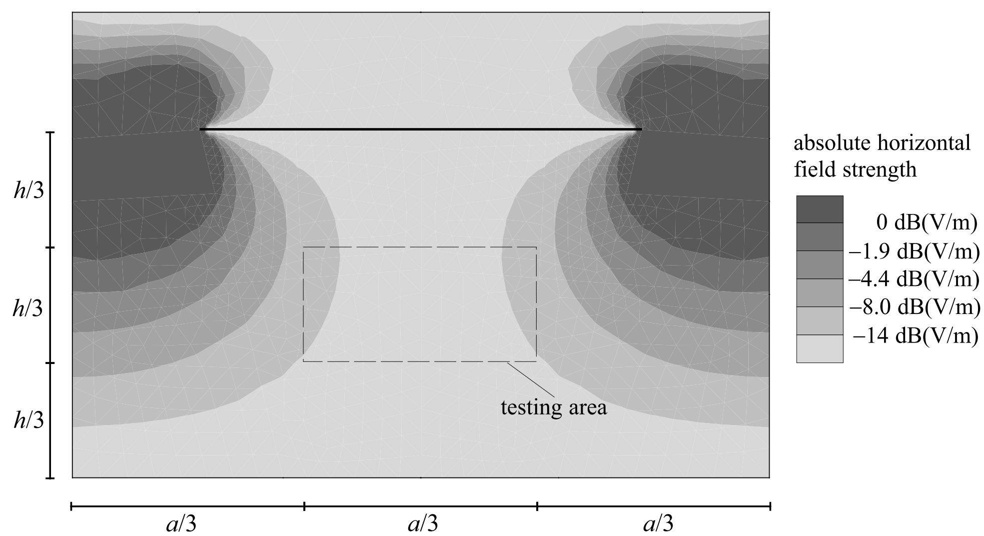

Figure 4.8: *The absolute value of the simulated horizontal field strength in the cross section of the cell.*

The measured field distribution in the cross section of the testing volume at 30 and 100 MHz is illustrated by a contour plot in figure 4.10. The results are obtained at an input power of 24.8 dBm where the expected nominal field strength is 20.5 dBV/m which corresponds well to the measured value in the center of the cross section which is 20.4 dBV/m. The measured field pattern is similar to the calculated one shown in figure 4.9. It must be noted though that for lower frequencies the deviations towards the upper and lower end of the testing volume are increasing.

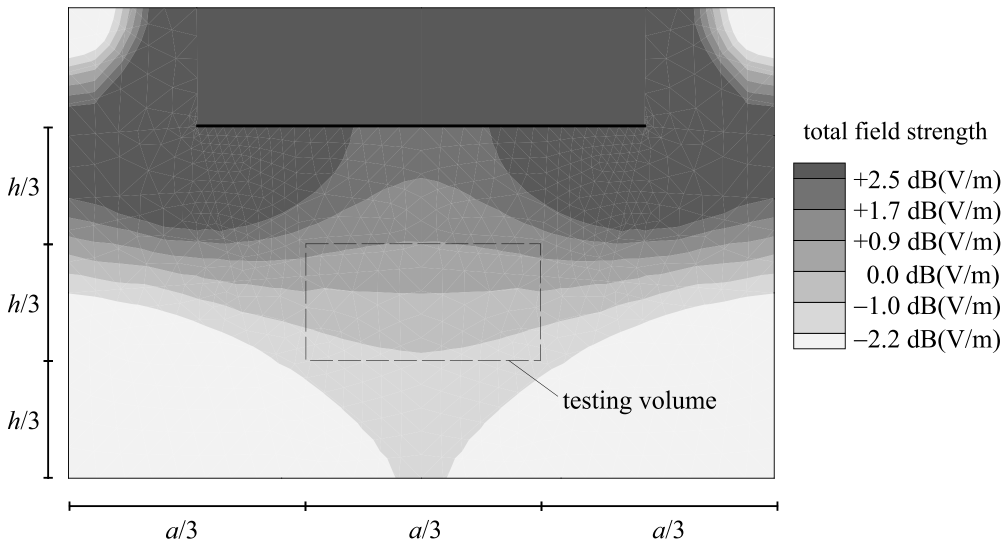

Figure 4.9: *The simulated total field strength in the plane of the cross section.*

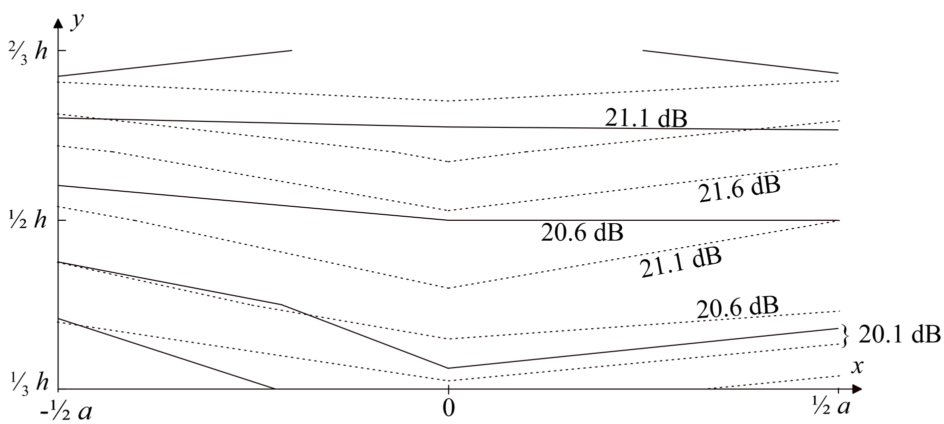

Figure 4.10: *The measured field strength pattern at 30 MHz (— — —) and at 100 MHz (—) in the cross section of the testing volume.*

In [18] research has been done on higher mode propagation and a comparison of simulated and measured field patterns within a GTEM cell are discussed. A good accuracy was stated for a two-dimensional electrostatic model that is similar to the one used in this work.

4.2 Emission measurements

In emission measurements the port of the cell is connected to the measuring equipment for monitoring the output power as a result of emissions from the tested equipment situated inside the testing volume. The equipment can be battery driven or use an external voltage supply connected via a special feed through with HF filters at the outer conductor. If needed, a unit to control the EUT can be connected through the feedthroughs as well.

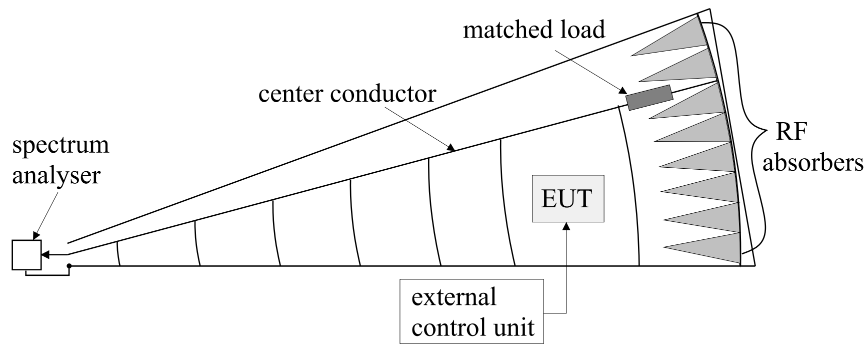

Figure 4.11: *For emission measurements the port is connected to the monitoring equipment. The EUT is either independent or uses an external voltage supply and/or a control unit.*

The GTEM cell acts as its own sensor and transmitter. Thus for emission measurements no antennas are needed to measure the strength of radiated fields arising from the EUT. However, the GTEM emission measurements results in output voltage data whereas in emission measurements described e.g. in the EMC standard IEC 1000-4-3 the radiated electric and magnetic field strength at 3 or 10 m distance is obtained through antennas. To compare GTEM results with data obtained from reference environments correlation methods have to be established.

One common method is described in [19], [20], [21] and [22]. The approach is to replace the EUT by a multi-pole model which would give the same radiation pattern outside some volume containing the source. The analysis is simplified, if the far-field pattern is considered and the source is electrically small. One needs then only to determine the leading terms of the multi-pole expansion to characterise the EUT sufficiently. The leading terms are the equivalent moments of the electric and magnetic dipoles. The radiation of both dipole types has been well considered. The resulting equations enable one to position such a dipole at any position over a ground screen and to compute the field strength e.g. at 3 m or 10 m distance, which is the typical setup according to IEC 1000-4-3. This is a valid alternative to OATSs or free space environments, subject to above mentioned limitations for the size of the EUT with respect to size and frequency.

4.3 Measurement results

In this section the results of two measurements are presented.

(a) The radiation pattern of a small antenna was measured at 1.885 GHz. The results were compared to those made in the antenna chamber of the Radio Laboratory of HUT to show a example of using the cell for antenna measurements.

(b) An electrically small noise radiator with was placed in the testing volume and the output voltage of the cell measured. The radiator, that generates radiation peaks every 10 MHz, was designed for a frequency range of about 500 MHz.

The results are compared to those made in a free space environment. The comparison should show the reliabilty of the cell above 300 MHz, where no calibration measurements as for the field uniformity were performed.

4.3.1 Small antenna

The H-plane field pattern of a $\lambda_G/4$ patch antenna (see figure 4.12) was measured at its reasonance frequency of 1.885 GHz.

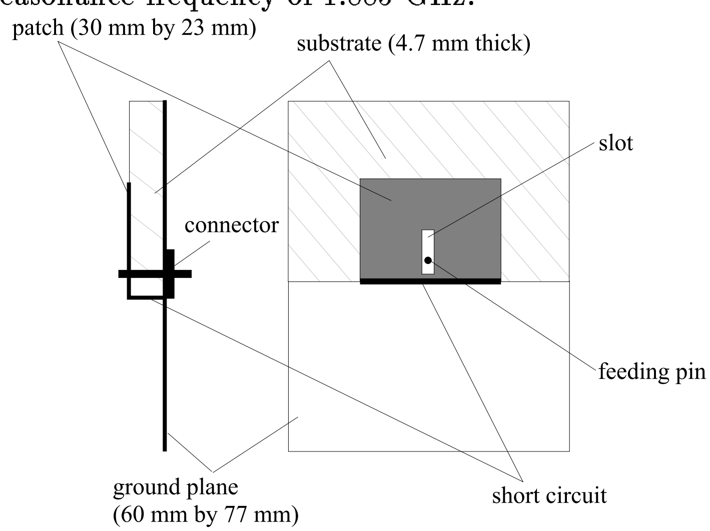

Figure 4.12: *The $\lambda_G/4$ patch antenna. The patch measures 30 by 23 by 4.7 mm.*

The antenna was situated in the center of the testing volume and rotated around its vertical axis. The power at the input of the antenna was 0 dBm and the output power of the cell was measured with the HP 8596E Spectrum Analyzer. The attenuations of cables were corrected.

For comparison the H-plane radiation pattern was measured in an anechoic room with a distance to the measurement antenna of 3 m also using the HP 8596E Spectrum Analyzer. The power at the input of the antenna was 7 dBm.

In figure 4.13 the H-plane radiation pattern obtained in the GTEM cell and in the antenna chamber is plotted against the angle about the vertical axis.

When measuring the front lobe the maximum output power of the GTEM cell was -24.6 dBm (corrected for the cabling) whereas in the anechoic chamber at 3 m distance -40 dBm (corrected for the cabling) were measured at the output of the receiving antenna. The gain of the receiving horn antenna for 1.885 GHz is $G_a = 9.2$ dB, i.e. an antenna factor of $AF = 19.77\text{dB} - 20 \cdot log(\lambda) - G_a[dB]$=26.5 dB$\frac{\mu V/m}{\mu V}$.

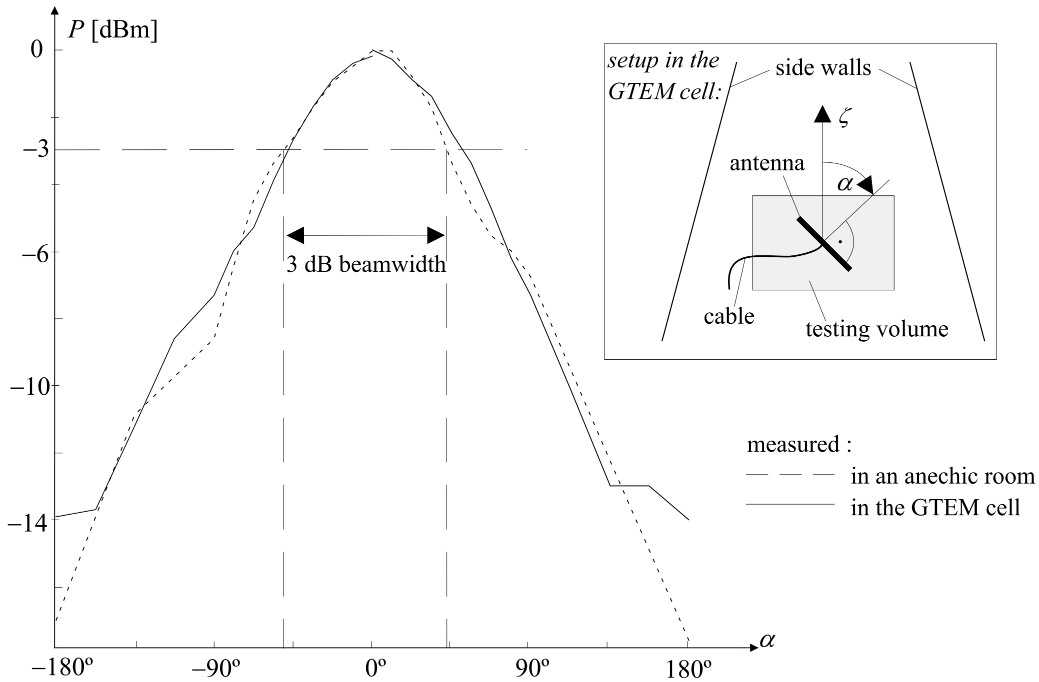

Figure 4.13: *The H-plane radiation pattern of a $\lambda_G/4$ patch antenna at 1.885 GHz measured in a shielded room (—) and in the GTEM cell (− − −) plotted against the angle about the vertical axis.*

The different environments show good correspondance in the measurement of the field pattern. A characteristic property of an antenna, the 3 dB beamwidth can in both environments be determined as about 90°.

The dynamic range of the cell can not exceed the reflection coefficient of the termination section. If the main lobe is more than e.g. 20 dB higher than the back lobe the reflections from the rear will influence the measurement of the back lobe.

In the measurments with the GTEM cell the values for $|\alpha| > 150°$ form a plateau 14 dB below the main lobe level. This might indicate, that the dynamic range is only about 14 dB although the reflection coefficient of the cell at 1.885 GHz is about $\Gamma = 23$ dB (see figure 3.19). However, Γ was determined with waves propagating in the TEM mode. The far field of the antenna can be compared to the TEM mode but in the small distance to the absorbers (= 10 cm) the electric field cannot be considered a perfect far field. The reflections from absorbers that are situated inside the near field are more likely to be higher than in the nominal case of a planar wave at normal incidence. Hereby the dynamic range of the measurement is decreased.

This shows a general problem of antenna measurements which might increase at lower frequencies, where the radius of the near field is even larger so that the matching of the termination section gets even worse. To investigate the usability of the GTEM cell for antenna measurements the reflection properties of the absorbers should be examined with help of an antenna with higher gain. This would increase the effect of the reflections on the measurements of the field pattern. The multi-pole method could be included into those investigations.

4.3.2 Noise radiator

A wide band generator with an antenna having electric dipole characteristic and producing spectral lines at harmonics of 10 MHz up to 1 GHz was measured in an free space environment with the *Chase* EMC antenna BILOG CBL61111 on the roof of the Department of Electrical Engineering of HUT. The distance above ground was 3 m as was the distance from the generator to the antenna. The device was a prototype, that was not yet optimized for its dipole characteristics so a orientation of the device was chosen with a maximum output power of the vertically polarised antenna. The output power was measured with the HP 8596E Spectrum Analyzer.

The generator was then situated in the center of the testing volume. The same cables and spectrum analyser were used as in the free space measurements to cancel out differences in the setup.

In figure 4.14 the levels of the spectral lines measured in both environments are plotted against the frequency without a correction of the attenuation of the cables. The relative vertical position of the scales was optimized for a small overall deviation.

In these measurements the output voltage of the GTEM cell was 69 dBμV when the field strength determined by the antenna at 3 m distance was 50μV/m.

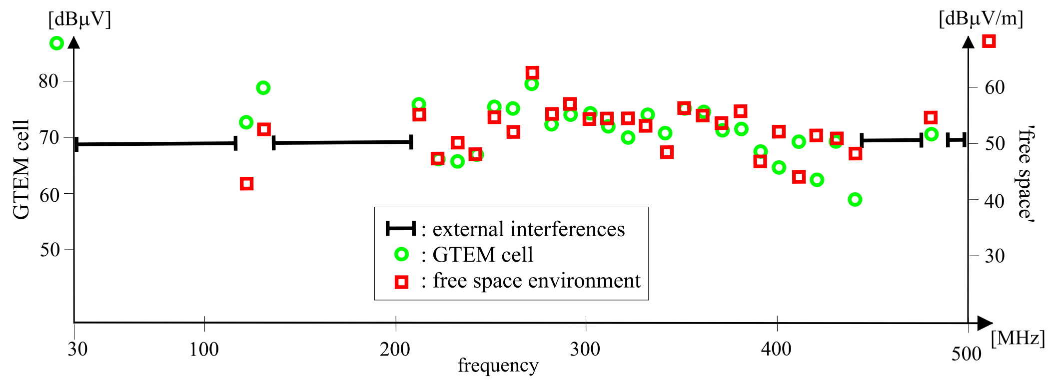

Figure 4.14: *The output voltage of the GTEM (◯) and of the EMC antenna (□) as a result of emissions from the test radiator. Some frequencies are blanked because of external interferences in the outside measurements.*

The frequencies, where external interferences disturbed the outside measurements were blanked. The remaining spectral lines show a correpondance of ± 2 dB except for around 120 and 420 MHz. Above 500 MHz the correspondance was not very good (see Appendix B), which might be due to a changing polarisation of the antenna inside the generator depending on the frequency. At higher frequencies cross-polarisations within the GTEM cell and the EMC antenna can be excited causing different results. The measurements should be continued with an improved generator with a better dipole characteristic.

5 Conclusions

The aim of this work was the design and the construction of a GTEM cell which can be used for radiated EMC measurements of small electronic equipment in a frequency range from 30 MHz up to at least 1 GHz according to international standards for EMC measurements. According to IEC 1000-4-3 [5] a field uniformity of ± 3 dB in position is required within the testing volume inside the GTEM cell. To achieve that limit the reflection coefficient of the termination section must be below -20 dB. As a function of frequency the field strength in the testing volume should not vary more than ± 3 dB. A nominal field strength inside the testing volume of at least 10 V/m should be possible.

The size of the cell was limited in order to ensure its portability. This has lead to a cell with a length of 2.2 m yielding in a testing volume with the dimensions 23 cm x 17 cm x 10 cm.

The GTEM cell is described as a transmission line operated in the TEM mode to simulate a free space plane wave. The theoretical background for the design of such a device is presented. Special attention is directed to the properties of of the hybrid termination section. Two different concepts of the current termination are described. Two possible methods for the determination of the characteristic impedance of an asymmetric rectangular transmission line are presented.

The construction of a GTEM cell is documented. Especially the design of the feed section and of the hybrid termination are documented and evaluated in detail through TDR measurements and measurements of the reflection coefficient. Problems in the matching of the current termination at $20 - 80$ MHz lead to a return loss smaller than 20 dB. Nevertheless a field uniformity of better than ± 3.5 dB in position is achieved for $10 - 100$ MHz and better than ± 2 dB at $100 - 300$ MHz. A nominal field strength inside the testing volume of over 30 V/m can be achieved with an input power of $P_{in} = 3$ W.

The application of the GTEM cell in radiated susceptibility tests and measurements of radiated and conducted emissions is described. Finally the results of two application measurements are presented.

First, the H-plane field pattern of a $\lambda_G/4$ patch antenna was measured at a frequency of 1.885 GHz. The beamwidth of the antenna could in both cases be determined as $90°$. Hereby a possibility to use the GTEM cell for certain antenna measurements is indicated. However, problems like the limited dynamic range of the GTEM cell are pointed out.

Second, the radiation of a small noise radiator with a frequency range of $10 - 1000$ MHz was measured with the GTEM cell and in a free space environment and the results compared. The frequency response in both environments show a fairly good correspondance up to 500 MHz. Measurements should be repeated with an improved generator as for its dipole characteristic.

From the antenna measurements a factor could be defined for the GTEM cell, that could be interpreted as an effective distance related to free space environments. In a free space environment a transmitter situated at the effective distance from an antenna with $G_a = 1$ results in the same output voltage at both GTEM cell and receiving antenna. Further investigations with the attention to antenna measurements but using the multi-pole model that was described in chapter 4 should be done. Therefore more calibration measurements in a wide frequency range (up to 2.5 GHz) are suggested.

The shielding properties of the cell should be verified and improved if necessary. The termination region should be improved for its absorption properties at 20–80 MHz in order to achieve higher field uniformity for the low frequencies. A new approach for the tapering of the teeth should be done. The influence of the absorbers on the characteristic impedance can be approximated on the basis of the knowledge of the complex permittivity at least for a single frequency (30 MHz).

Bibliography

[1] M.L. Crawford "Generation of standard EM fields using TEM transmission cells" *IEEE Transactions on Electromagnetic Compatibility* Vol. EMC-16, No.4, November 1974, pp.189-195.

[2] M.L. Crawford, J.L. Workman, C.L. Thomas "Expanding the Bandwidth of TEM cells for EMC measurements" *IEEE Transactions on Electromagnetic Compatibility* Vol. EMC-20, No.3, August 1978, pp.368-375.

[3] D. Königstein, D. Hansen "A New Family of TEM-cells with Enlarged Bandwidth and Optimized Working Volume" *Proceedings of the 7th International Zurich Symposium on Electromagnetic Compatibility* Zurich, March 1987, pages 127-132.

[4] D. Hansen, P. Wilson, D. Königstein, H. Schaer, "A broadband alternative EMC test chamber based on a TEM-cell anechoic-chamber hybrid concept" *Proceedings of the 1989 International Symposium on Electromagnetic Compatibility* (Nagoya), September 1989, pages 133-137.

[5] "Electromagnetic Compatibility (EMC) - Part 4: Testing and Measurement Techniques - Section 3: Radiated, Radio- Frequency, Electromagnetic Field Immunity Test", *International Standard CEI/IEC 1000-4-3*, Geneva, February 1995.

[6] "Limits and Methods of Measurement of Radio Interference Characteristics of Information Technology Equipment", *International Electrotechnical Commission, International Special Committee on Radio Interference*, European standard EN 55 022, Brussels, June 1987.

[7] M.L. Crawford, J.L. Workman, "Predicting free-space radiated emissions from electronic equipment using TEM cell and open-field site measurements", *IEEE Symposium on Electromagnetic Compatibility*, Baltimore, 1980, pp.80-85.

[8] I. Sreenivasiah, D.C. Chang, M.T. Ma, "Emission characteristics of electrically small radiating sources from tests inside a TEM cell", *IEEE Transac-*

tions on Electromagnetic Compatibility Vol. EMC-23, No.3, August 1981, pp.113-121.

[9] D. Hansen, D. Königstein, "Vorrichtung zur EMI-Prüfung elektronischer Geräte" *Patentschrift bei der Schweizerischen Eidgenossenschaft*, CH 670 174 A5, Mai 1989.

[10] E. Yamashita, K. Atsuki "Strip line with rectangular outer conductor and three dielectric layers" *IEEE Transactions on Microwave Theory and Techniques* Vol.18, No.5, May 1970, pp.238-244.

[11] R. De Leo, T. Rozzi, C. Svara, L. Zappelli, "Rigorous analysis of the GTEM cell", *IEEE Transactions on Microwave Theory and Techniques* Vol.39, No.3, March 1991, pp.488-499.

[12] P.F. Wilson "Higher-order mode field distribution in asymmetric TEM cells" *International Symposium on EM Theory, URSI*, Stockholm, August 1989, pp.108-110

[13] R. De Leo, L. Pierantoni, T. Rozzi, L. Zappelli, "Wideband analytical model of the GTEM cell termination", *Proceedings of the 11th International Zurich Symposium and Technical Exhibition on Electromagnetic Compatibility* , March 1995, pp.607-612.

[14] T. Rozzi, R. De Leo, L. Pierantoni, G. Gerini, "A simplified analytical model of the termination of a GTEM cell", *Proceedings of the 1994 International Symposium on Electromagnetic Compatibility* (Rome), September 1994, pp.235-239.

[15] P.A. Chatterton, M.A. Houlden, *EMC; Electromagnetic theory to practical design*, J. Wiley & Sons, Liverpool, May 1991.

[16] R.E. Collin *Foundations for Microwave Engineering*, McGraw-Hill, Kogakusha, 1966, p. 239.

[17] D. Weiss "A user's insight into radiated emission testing with GTEM cells", *IEEE International Symposium on Electromagnetic Compatibility*, Cherry Hill, August 1991, pp.157-162.

[18] D. Hansen, D. Ristau, T. Spaeth, W.A. Radasky, K.S. Smith, J.L. Gilbert, "Analysis of the measured field structure in a GTEM 1750", *IEEE International Symposium on EMC*, Chicago 1994, pp.144-149.

[19] D. Hansen, P. Wilson, D. Königstein, "Simulating Open Area Test Site emission eeasurements based on a novel broadband TEM cell", *Proceedings of the IEEE 1989 National Symposium on Electromagnetic Compatibility*, Denver, May 1989, pp.171-177.

[20] P. Wilson, D. Hansen, H. Hoitink, "Emission measurements in a GTEM cell: simulating the free space and ground screen radiation of a test device", *ABB research report CRB 89007C*, Baden, June 1988.

[21] D. Hansen, P. Wilson, D. Königstein, H. Garbe, "Emission and susceptibility testing in a tapered TEM cell", *Proceedings of the 8th international Zurich Symposium and Technical Exhibition on Electromagnetic Compatibility*, Zurich, March 1989, pp.227-232.

[22] M.J.Thielberg, E.L. Bronaugh, J.D.M. Osburn, "GTEM to OATS radiated emissions correlation from 1-5 GHz", *IEEE International Symposium on EMC*, Chicago 1994, pp.387-392.

[23] Antenna factor listing of the Chase Bilog CBL61111 Antenna, ser.no. 11966P.

Appendix A

The electric field strength was measured at three horizontal planes inside the testing volume (i and ii), in the vertical cross section through the center of the testing volume parallel to the rear wall (iii) and on a longitudinal axis between the inner and the bottom outer conductor.

The results are given in three forms: (1) the reading from the analog scale of the meter, (2) the corresponding field strength in V/m according to the calibration and (3) the field strength in dBV/m.

The scale of the meter is proportional to the square of the field strength. The meter was calibrated for a field strength of 10 V/m with the following readings:

10 MHz:	6.2
30 MHz:	6.8
60 MHz:	6.8
80 MHz:	6.7
100 MHz:	6.5
140 MHz:	6.6
180 MHz:	6.3
230 MHz:	6.0
300 MHz:	5.5

Appendix B

The radiated spectrum of the noise generator measured with help of the GTEM cell and in an free space environment. The results from the free space environment are corrected for the antenna factor of the bilog antenna [23]. The cables were the same in both setups and the attenuation can be linearily approximated by -(0.5+2.2·f/GHz)dB.